An investigation into reducing the uncertainties associated with the leading order hadronic contributions to the anomalous magnetic moment of the muon

by

Andrew Carroll

September 2013

Abstract

Comparison between theoretical calculations of the anomalous magnetic dipole moment of the muon and its experimentally measured value provide one of the most accurate tests of the standard model and possibly the only current indication of beyond the standard model physics. The disagreement between theory and experiment at the time of writing is 3.4 standard deviations.

The errors in the theoretical calculation of the anomalous magnetic moment are dominated by those arising from the hadronic sector. Due to asymptotic freedom, perturbative QCD is inapplicable at low energies, meaning that calculations at these energies must utilise experimental cross sections. This requires processing and synthesising data from many different experiments and using this data to predict a low energy, hadronic contribution to the anomalous magnetic moment of the muon.

In order to investigate this discrepancy further, one must examine and attempt to reduce the uncertainties in the data. Many of these uncertainties are unavoidable experimental or statistical errors, but a large proportion of the errors arise as a result of the combination of different data sets from different experiments, in particular how the different experiments accounted for radiative corrections. In this project an investigation is undertaken into how the various experiments dealt with the radiative corrections and how one might decrease the uncertainty in the anomalous magnetic moment measurement by formulating a procedure to categorise which data sets should be included and which not.

In this project, the author's contribution was to recalculate the FSR correction factor using an experimentally dependant regulator. Relations were then found relating the regulator to experimental angular cuts, allowing one to calculate the required FSR correction factor for individual experiments, rather than simply including half of the inclusive eta factor. The applications of this procedure in this project are to the K^+K^- channel.

Contents

Table of Contents

Acknowledgements

I would like to thank my supervisors Steve Maxfield and Thomas Teubner, who have both been enormously patient and wise mentors over the last year. I would also like to thank Themis Bowcock, who gave me the chance to participate in this exciting experiment in a year that might otherwise have been wasted.

Chapter 1

Introduction

1.1 The anomalous magnetic moment

The quantum mechanical magnetic dipole moment, $\vec{\mu}$,of a fundamental particle is defined by the equation

$$\vec{\mu} = -g\mu_B\vec{S} = -g\frac{e}{2m}\vec{S},$$

where g is the gyromagnetic factor or g-factor of the particle, e the charge associated with the particle, m its mass, $\vec{S}$ its spin and μ_B is the Bohr magneton. This equation is therefore a relation between how the spin angular momentum of a point particle, coupled with its charge, lead it to have a dipole moment which will cause it to interact with a magnetic field, most famously in the case of the Stern-Gerlach experiment. The g-factor for spin half particles is a dimensionless constant of proportionality and predicted to be exactly 2 by the Dirac equation. Taking the non-relativistic limit of the Dirac equation, (see reference (1)), one finds the Pauli equation, familiar from non-relativistic quantum mechanics,

$$i\frac{\partial\psi}{\partial t} = \left[\frac{1}{2m}\left(\vec{p} - e\vec{A}\right)^2 - \frac{e}{2m}\vec{\sigma}\cdot\vec{B} + e\Phi\right]\psi\,.$$

Here, ψ is the two component Pauli spinor, $\vec{p}$ the momentum, $\vec{A}$ the electromagnetic vector potential, Φ the scalar potential, m the mass of the fermion, e its charge, $\vec{\sigma}$ are the Pauli matrices and $\vec{B}$ is the magnetic field. Expanding the square brackets out gives

$$i\frac{\partial\psi}{\partial t} = \left[\frac{\vec{p}^2}{2m} + \frac{e}{2m}\left(-\vec{p}\cdot\vec{A} - \vec{A}\cdot\vec{p}\right) + \frac{e^2}{2m}\vec{A}^2 - \frac{e}{2m}\vec{\sigma}\cdot\vec{B} + e\Phi\right]\psi\,.$$

Using the equations

$$-\vec{p}\cdot\vec{A} - \vec{A}\cdot\vec{p} = -\vec{L}\cdot\vec{B},$$

where L is the orbital angular momentum, and

$$\vec{S} = \frac{1}{2}\vec{\sigma}$$

one finds

$$i\frac{\partial \psi}{\partial t} = \left[\frac{\vec{p}^2}{2m} + \frac{e}{2m}\left(-\vec{L}\cdot\vec{B}\right) + \frac{e^2}{2m}\vec{A}^2 - \frac{2e}{2m}\vec{S}\cdot\vec{B} + e\Phi\right]\psi\,.$$

Rearranging gives the equation

$$i\frac{\partial \psi}{\partial t} = \left[\frac{\vec{p}^2}{2m} - \frac{e}{2m}\left(\vec{L} + 2\vec{S}\right)\cdot\vec{B} + \frac{e^2}{2m}\vec{A}^2 + e\Phi\right]\psi\,.$$

The first term in the right hand side bracket is the non-relativistic kinetic energy of the free spin half particle, the second the interaction of the spin of the particle with an external magnetic field, the third the interaction of the particle and the vector potential, and the fourth the interaction with the scalar potential. It is straightforward to now redefine the quantity in brackets as

$$H = H_0 + H_{int}\,,$$

where the second term on the right hand side corresponds to the interaction component of the Hamiltonian. The interaction Hamiltonian is then rewritten as

$$H_{int} = -\frac{e}{2m}\left(\vec{L} + 2\vec{S}\right)\cdot\vec{B} + \frac{e^2}{2m}\vec{A}^2 + e\Phi.$$

The energy of the interaction between a spinning charge and a magnetic field is defined to be of the form

$$H = -\vec{\mu}\cdot\vec{B},$$

where $\vec{\mu}$ represents magnetic moment, accounting for both orbital and spin angular momentum contributions. This then allows one to split up the interaction Hamiltonian further to give

$$H_{int} = -\frac{e}{2m}\vec{L}\cdot\vec{B} - \frac{e}{2m}2\vec{S}\cdot\vec{B} + \frac{e^2}{2m}\vec{A}^2 + e\Phi = \vec{\mu}_{orbit}\cdot\vec{B} + \vec{\mu}_{spin}\cdot\vec{B} + \frac{e^2}{2m}\vec{A}^2 + e\Phi\,,$$

where $\vec{\mu}_{orbit}$ and $\vec{\mu}_{spin}$ are the orbital angular momentum and spin angular momentum magnetic dipole moments respectively. As mentioned above, the spin magnetic moment for a fundamental particle obeys the equation

$$\vec{\mu}_{spin} = -g\mu_B\vec{S}.$$

The Bohr magneton has the form

$$\mu_B = \frac{e}{2m}.$$

For this to hold one must therefore have

$$\vec{\mu}_{spin} = -g\mu_B\vec{S} = -g\frac{e}{2m}\vec{S} = \frac{e}{m}\vec{S},$$

where the last step comes from a comparison with the interaction Hamiltonian above. This leads finally to the conclusion

$$g = 2,$$

showing that the Dirac equation gives a gyromagnetic factor of exactly two.

This result is replicated in QED by the contributions from the lowest order diagrams, but loop corrections change this value slightly, so that for instance the modern gyromagnetic factor value for the electron is approximately 2.002. This difference between the prediction of the g-factor for a lepton from the Dirac equation, and the actual value when vacuum polarization (VP) and other corrections are accounted for, is referred to as the anomalous magnetic dipole moment a_l and is defined to be

$$a_l = \frac{g_l - 2}{2},$$

where l is a subscript denoting an electron, muon or a tau. The anomalous magnetic dipole moment is an extremely important and famous quantity in particle physics for two reasons. Firstly, it is one of the most accurately measured experimental values, allowing an extraordinarily accurate comparison between experiment and theory and leading, in the case of the electron, to one of the most precisely measured quantities in all of science. Secondly, due to this extreme precision, one may use the anomalous magnetic moment

measurements to search for physics beyond the standard model. For instance, as yet undiscovered quantum fields would manifest as additional VP contributions and hence alter the anomalous dipole moment value, leading to a contradiction between theory and experiment. This could be used as an experiment to detect, amongst other things, supersymmetric particles, showing how the extraordinary precision possible in measuring the anomalous dipole moment makes it very much still an important experiment in the age of the supercollider (see chapter 5 for more details).

In 1956 Beresetskii (2) noted that sensitivity of a_l to new physics is mass dependent and takes the form

$$\delta a_l \sim \left(\frac{m_l}{M}\right)^2 \quad (M \gg m_l)$$

where M is some new physics energy scale which we can set to be much greater than the masses of any of the three presently known charged leptons, as an experimental fact. The term energy scale is somewhat more general than simply the mass of an unknown particle, also accounting for hypothetical heavy states or a cut-off beyond which the standard model loses its validity. What this equation shows is that, between the three charged lepton types, the sensitivity scales as a quadratic function of the mass. One may easily show that, *ceteris paribus*, the muon is more sensitive to new physics than the electron by the ratio of their masses squared, or approximately 40,000. One must balance this increased intrinsic sensitivity of the muon over the electron against the greater experimental precision possible when measuring the anomalous magnetic moment of the electron than the muon. As of November 2011, the anomalous magnetic moments of the electron and muon respectively are:

$$a_e^{exp} = 11596521.8073\ (0.0028) \times\ 10^{-10}\ [0.24\ ppb]\ (3)$$

$$a_\mu^{exp} = 11659208.9\ (6.3) \times\ 10^{-10}\ [0.54\ ppm]\ (4)\ .$$

Making the experimental measurement of a_e a factor of 2000 times more accurate than a_μ. This is an order of magnitude smaller than the improved sensitivity of the muon to new physics, making the muon the better choice for probing physics beyond the standard model.

Chapter 2

The g-2 experiment

1.1 Experimental description

The g-2 experiment is a high precision experiment which will attempt to measure the anomalous magnetic moment of the muon and look for deviations from theory, hinting at physics beyond the standard model. Located at Fermilab's muon campus, the experiment will use the Fermilab accelerator complex to produce a high intensity beam of muons, which will then enter a superconducting magnet, decay, and the anomalous magnetic moment measured. With a planned four-fold increase in the accuracy of the experiment, the g-2 experiment will be able to measure the anomalous moment to one part in 10 million, making it more sensitive to new physics than any previous experiment of its kind.

Hints at new physics were found at its predecessor, the E821 experiment at the Brookhaven National Laboratory, which found a statistically significant deviation (approximately 4 sigma (5)) from theoretical predictions. In order to further investigate this discrepancy, the superconducting magnet was moved from Long Island in New York to Chicago, Illinois, where the Fermilab accelerator complex will create a beam of muons more intense and pure than previously utilised in order to increase the statistics and therefore the precision of the measurement.

The muons are stored in a 50-foot-diameter, 700 ton storage ring. The storage ring is constructed as one continuous iron magnet, which is in turn further magnetised by the surrounding superconducting coils. The magnet is C-shaped in profile, to facilitate the passage of the decay-produced electrons to the detectors, and has essentially two parts, the yoke and the poles. The yoke makes up the bulk of the magnet and so are made from conventional AISI 1006 iron, whereas the poles, which sit above and below the muon beam and are required to be very pure due to their domination of the field aberrations, are made from continuous cast steel. The storage ring is cooled with two-phase helium flowing through tubes attached to the coils. The time it takes to cool the magnet down from 300K to 4.9K takes typically around 10 days. The ring is surrounded by three superconducting coils which provide the 1.45 Tesla magnetic field. One coil is placed at the outer radius to drive the field across the storage ring gap, and two coils are placed at the inner radius, above and

below the midplane, to cancel the flux in the ring centre and improve the field homogeneity. These coils are made of titanium-niobium filaments in a copper matrix, surrounded by ultra-pure aluminium. The coils are powered by a low voltage supply, providing 5200 A of current.

Figure 1: Photograph of the g-2 ring located at Brookhaven National Laboratory

This magnetic field constrains the 3.1 GeV muons to move in a circular orbit of radius 7.112 meters. The storage region has a cross sectional diameter of 9 cm. In order to achieve the extraordinary precision required, the magnetic field strength must be known extremely well, requiring that the average field strength be uniform to one part per million over the muon storage aperture. To make the magnetic field homogenous, one must 'shim' the magnets. Shimming is a collection of techniques used to alter the magnetic field; for instance, one may insert aluminium shims between the yoke and the poles, or tilt the poles themselves. Shimming is used in conjunction with NMR, which utilises a spherical water sample to measures the field in terms of the proton spin precession frequency, and Hall probes where NMR was not viable (6) (7).

1.2 g-2 measurement of a_μ

The measurement of the anomalous moment of the muon at CERN and by the g-2 experiment at the Brookhaven National Laboratory both utilised a storage ring to determine the spin precession of muons travelling in a circular orbit. A proton beam, consisting of $\approx 60 \times 10^{12}$ protons per 2.5s cycle, each with energy of approximately 24 GeV, are produced by an Alternating Gradient Synchrotron or AGS and fired at a target to produce pions, of mass about 140 MeV. The target is preferably one that produces copious amounts of pions when a proton beam is incident upon it. The target chosen for this purpose at the g-2 experiment is Nickel, with a thickness of about 1 interaction length[1].

The pions which are produced are then momentum selected and allowed to decay, with a decay ratio of approximately 99.98% (8) of the pions decaying to muons. These muons are once again momentum selected before being fed into the storage ring. Due to parity violation of the weak interaction, the direction of the spin and momentum of the muons are identical when they are created.

The differential decay rate of the muon in its rest frame is given by the equation

$$\frac{d\Gamma}{d\Omega} = N(E_e)\left(1 + \frac{1-2x_e}{3-2x_e}\, cos\,\theta\right),$$

where E_e is the positron energy, x_e is the positron energy in units of the maximum energy $m_\mu/2$, $N(E_e)$ is a normalisation factor and θ is the angle between the positron momentum in the muon rest frame and the direction of spin of the muon (8). The factor

$$A(E_e) \equiv \frac{1-2x_e}{3-2x_e}$$

is called the asymmetry factor . This factor strongly peaks spectrum at small θ, meaning that the positrons are strongly focused in the direction of the muon spin. Physically, this factor is a manifestation of the parity violation exhibited in this process.

Due to Larmor precession, the magnetic field will cause the momentum and spin vectors to decouple and the spin vector will precess with a frequency ω_s. In addition, in order to keep

[1] The interaction length is defined as the mean path length required to reduce the energy of the charged particles in the beam by a factor of 1/e.

the muons focused in the plane transverse to the magnetic field, one must apply a quadrupole electric field which will also affect the muon spin precession. The amount by which the orbital frequency and the spin precession frequency decouple is given by

$$\omega_a = \omega_s - \omega_c$$

where ω_c is the synchrotron frequency and ω_s is the spin precession frequency. The decoupling frequency is given by

$$\vec{\omega}_a = \frac{e}{m_\mu}\left[a_\mu \vec{B} - \left(a_\mu - \frac{1}{\gamma^2 - 1}\right)\vec{v} \times \vec{E}\right],$$

where $\vec{v}$ is the muon velocity. In order to simplify this equation, one can tune the gamma factor so that both the terms in the round brackets are equal. This then results in what is called the magic energy E_{magic} having a value of approximately 3.1 GeV. Setting the muon energy to this magic value simplifies the above equation, removes the electric field contribution and so minimises errors arising from any uncertainty in the electric field value. Inserting the magic energy into the above equation gives

$$\omega_a = \frac{e}{m_\mu} a_\mu B \, .$$

In addition, the gamma factor value of around 30 increases the muon decay time from about 2μs to about 60μs, allowing more oscillations before decay and hence improving accuracy. Parity violation also causes the electrons, into which the muon decays, to be preferentially emitted in the direction of the spin of the muon, hence allowing precession measurement. It is therefore clear that measurement of the direction at which the electrons are emitted, combined with the above equation, can be used to measure the anomalous magnetic moment of the muon.

In order to measure the decoupling frequency and relate it to the anomalous magnetic moment, one must measure the magnetic field. This is done via nuclear magnetic resonance (NMR). The g-2 experiment utilises a H_20 probe, which relates the magnetic field to the magnetic moment of a free proton, via the equation

$$B = \frac{\omega_p}{2\mu_p} .$$

where ω_p is the spin precession angular velocity of a proton in water, and μ_p the magnetic moment of a free proton. Combining this equation with the previous equation for ω_a gives

$$a_\mu = \frac{\omega_a \mu_p}{\omega_p} \frac{2m_\mu}{e}.$$

One then employs the equation

$$a_\mu = \frac{2m_\mu}{e} \mu_\mu - 1$$

to remove the group of constants in the first equation for $a_\mu$and, after some brief rearranging, one finds

$$a_\mu = \frac{R}{\lambda - R},$$

where

$$R = \frac{\omega_a}{\omega_p} \text{ and } \lambda = \frac{\mu_\mu}{\mu_p}.$$

The constant λ is found via measurements of the microwave spectrum of ground state muonium. The value used by the g-2 experiment to calculate a_μ is

$$\lambda = 3.18334539(10)\ (30\ ppb).$$

Since the measurements of the spin precession frequency are very accurate, attaining a measurement accurate enough to compare with theoretical calculations tends to hinge on creating and measuring as homogenous a magnetic field as possible (see section 1.1).

1.3 Comparison of previous measurements of a_μ with prediction

Figure 2 is a graphic comparison between the measured value of the anomalous magnetic moment of the muon, and the predictions from the standard model made by various collaborations. This includes the predictions from Hagiwara, Martin, Nomura and Teubner (HMNT) in 2006 (9), those from Jegerlegner and Nyffeler in 2009 (10), Davier et al from 2010 (11), Jegerlehner and Szafrom from 2011 (12), and Hagiwara, Liao, Martin, Nomura and Teubner (HLMNT) from 2010 and 2011 (4)[2]. These are compared with the measurements from Brookhaven National Laboratory, where the second 'shift in lambda' measurement arises from the fact that Codata (The Committee on Data for Science and Technology) shifted their muon to proton magnetic ratio lambda (see section 1.2).

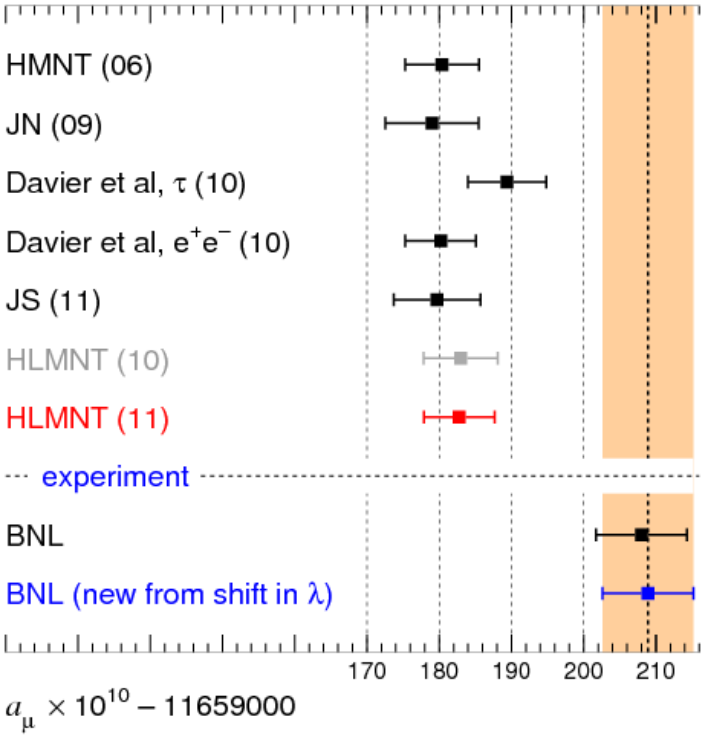

Figure 2: Comparison of various predictions of the anomalous magnetic moment, compared with the measurements made at Brookhaven National Laboratory

Taking the most recent HLMNT calculation gives a SM prediction of

$$a_\mu^{SM} = (11\,659\,182.8 \pm 4.9) \times 10^{-10}\,.$$

[2] Calculations using the decay of tau particles into pions and exploiting isospin symmetry to find the spectral function and hence the hadronic VP contributions, such as those used by Davier et al, are not considered in this work.

The lambda shifted value of the experimental value of the anomalous magnetic moment is

$$a_{\mu}^{exp} = 116\ 592\ 089(63) \times\ 10^{-11}\ ,$$

leading to a discrepancy of

$$a_{\mu}^{exp} - a_{\mu}^{SM} = (26.1 \pm 8.0) \times\ 10^{-10}.$$

This is equivalent to a 3.3 sigma disparity between the experimental and theoretical values.

Chapter 3

Calculation of a_μ

2.1 Contributions to the theoretical a_μ value

The theoretical value of the anomalous magnetic moment of the muon is a sum of the contributions from the possible virtual particles that could exist in the higher order diagrams of the fundamental vertex:

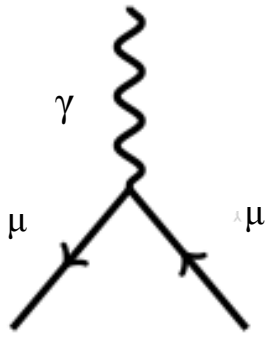

Figure 3: The QED fundamental vertex. In this case the photon is real, with virtual corrections applied at higher orders from the QED, EW and hadronic sectors.

The theoretical prediction for a_μ is therefore given by the equation:

$$a_\mu^{theory} = a_\mu^{QED} + a_\mu^{EW} + a_\mu^{had} + a_\mu^{new\ physics},$$

where the new physics component is included to account for any statistically significant discrepancy found between theory and experiment. It is this component which will allow one to detect the presence of beyond the standard model physics. The creation of particles which have not been accounted for in the calculation will affect the (experimental) anomalous moment value and lead to a discrepancy. The standard model makes a prediction of the value of the anomalous moment, accurate to 400 parts per billion. The g-2 experiment at Fermilab is expected to be able to measure the value to an accuracy of 140 parts per billion (13). This should then settle the matter of whether or not what was spotted at the g-2 experiment in Long Island was a statistical aberration or if it hails a new age in physics.

2.2 QED contributions to a_μ value

The QED component of the anomalous magnetic moment is known to an astonishing five loop accuracy (14). This contribution has the theoretical value

$$a_\mu^{QED} = (11658471.8951 \pm 0.008) \times 10^{-10}.$$

The error on this value is clearly very small and so one can have high degree of confidence that the QED contributions to a_μ are represented within this value.

2.2 EW contributions to a_μ value

The electro-weak contribution, which includes the diagrams containing the Z, $W^\pm$ and H bosons, has been calculated to two loop accuracy and is shown below (15):

$$a_\mu^{EW} = (15.36 \pm 0.1) \times 10^{-10}.$$

The latest evaluation of the electroweak contribution has recalculated the value with the recently obtained Higgs mass, Higgs contributions entering at the two-loop diagram level. This contribution is obviously much smaller than that from QED and, coupled with the fact that this value has been found consistently by several independent calculations, suggests that any electro-weak errors are under control.

2.4 Hadronic contributions to a_μ value

The largest error contributions in the calculation of a_μ are from the hadronic calculations, with associated uncertainties far larger than both those from QED and EW. This arises essentially from the fact that perturbative QCD cannot be used to calculate those diagrams which contain virtual low-energy loops. It is, however, precisely these low q^2 contributions that dominate the loop integrals, prohibitively damaging the capability for theoreticians to calculate the hadronic contributions to sufficient accuracy. One must therefore utilise a semi-phenomenological method involving data from e^+e^- annihilation experiments.

The hadronic a_μ component is conventionally split up into three separate pieces

$$a_\mu^{had} = a_\mu^{LOVP} + a_\mu^{HOVP} + a_\mu^{LbL},$$

where LOVP denotes the leading order vacuum polarisations contribution, HOVP the higher vacuum polarisations and LbL the light by light scattering contribution, representations of which are shown in figure 4.

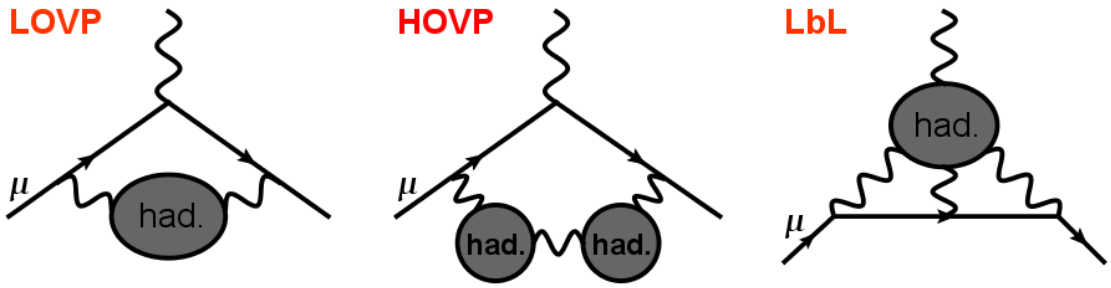

Figure 4: Feynman diagrams displaying the three classes of hadronic contributions to the anomalous magnetic moment.

LOVP and HOVP are both calculated using the semi-phenomenological method mentioned above, but the LbL calculations are model-dependent. Non-perturbative hadronic corrections to the photon propagator require the total bare cross section (16)

$$\sigma^0_{had}(s) = \sigma^{tot}_0(e^+e^- \to \gamma^* \to hadrons)\,,$$

where a bare cross section is one which includes no vacuum polarizations corrections or QED initial state radiation (ISR) corrections, but final state radiation (FSR) corrections are still present. This is often then reformulated as

$$R(s) = \frac{\sigma^0_{had}(s)}{\sigma_{pt}(s)} \quad , \quad \sigma_{pt}(s) = \frac{4\pi\alpha^2}{3s},$$

and $\alpha = \alpha(0)$. Combining this with the optical theorem and demanding analyticity gives the equation

$$a_\mu^{had,LO} = \left(\frac{\alpha m_\mu}{3\pi}\right)^2 \int_{s_{th}}^{\infty} ds\, \frac{R(s)K(s)}{s^2}\,.$$

This equation gives the anomalous magnetic dipole moment for the leading order hadronic contributions. The function $K(s)$ is called the kernel and increases monotonically from 0.4 at $m^2_{\pi^0}$ to 0.63 at $s = 4m^2_\pi$ and then approaches 1 as s approaches infinity. Due to the fact that perturbative QCD cannot be used below the heavy flavour threshold, one must insert

experimentally measured cross sections, corrected to bare cross sections, into the above equation in order to calculate $a_\mu^{had,LO}$.

As mentioned above, the insertion of the bare cross section into the equation for the calculation of the anomalous moment of the muon requires that the cross section value not include either ISR from QED or vacuum polarization corrections, but include FSR corrections. This requires the correction of the experimental data.

The reason vacuum polarization corrections are not wanted in the experimental cross section is to avoid double counting. This is because, if a virtual bubble was included in one of the Feynman diagrams for the process, say

$$e^+e^- \to \gamma^* \to \pi^+\pi^-,$$

then the contribution from this diagram to the cross section would be the same as the identical diagram in the next-to-leading order corrections to the anomalous moment, and so this diagram would have been accounted for twice, leading to double counting.

The simplest way to correct the data to remove vacuum polarization corrections is to multiply the cross section by the correction factor

$$C_{vp} = C_{vp}^A = \left(\frac{\alpha}{\alpha(s)}\right)^2,$$

which of course acts to replace the running coupling constant with its low energy counterpart, thereby removing any polarization contributions which are the reason for the fine structure constant having an energy dependence.

In those experiments in which the process ($e^+e^- \to \gamma^* \to \mu^+\mu^-$) was used to normalise the cross section, the corrections to the photon propagator cancel and so the correction factor is equal to unity:

$$C_{vp}^B = 1.$$

This is not the case for most experiments, however, which normalise via the Bhabha scattering process. If the normalisation cross section has not been vacuum polarization

corrected, the correction factor is dominated by the t channel photon exchange amplitudes at t_{min}. This is caused by the Bhabha scattering cross section having the form

$$\frac{d\sigma}{dt} \propto \frac{\alpha^2}{t^2}$$

at small $|t|$. This leads to the replacement

$$\alpha^2 \to [\alpha(t_{min})]^2.$$

The correction factor therefore becomes

$$C_{vp}^{C} = \left(\frac{\alpha(t_{min})}{\alpha(s)}\right)^2,$$

where

$$t_{min} = \frac{-s(1-\cos\theta_{cut})}{2}.$$

In some cases, particularly from the old data, only the electron and muon contributions to the photon vacuum polarization function have been accounted for. If these data were normalised via muon-pair production, cancellation still occurs and correction factor B still applies, but otherwise the appropriate correction factor is

$$C_{vp}^{D} = \frac{\left(\frac{\alpha_l(s)}{\alpha(s)}\right)^2}{\left(\frac{\alpha_l(t_{min})}{\alpha(t_{min})}\right)^2},$$

where $\alpha_l(s)$ is the running coupling constant with only the electron and muon contributions. Similarly, for some of the older data only the electron contribution has been accounted for, and so one must use the correction factor

$$C_{vp}^{D} = \frac{\left(\frac{\alpha_e(s)}{\alpha(s)}\right)^2}{\left(\frac{\alpha_e(t_{min})}{\alpha(t_{min})}\right)^2}.$$

Further information about vacuum polarization correction factors and the table correlating corrections to individual experiments can be found in reference 1.

FSR corrections are applied to the $e^+e^- \to \gamma^* \to \pi^+\pi^-$ and $e^+e^- \to \gamma^* \to K^+K^-$ data. The FSR correction factor modifies the cross section by reinserting the contribution from those diagrams which contain either real or virtual FSR. The correction factor is

$$C_{fsr} = 1 + \eta(s)\frac{\alpha}{\pi}.$$

The function $\eta(s)$ will be discussed in more detail later. This equation assumes point-like pions and kaons, an assumption which is expected to be valid near the $\pi^+\pi^-$ and K^+K^- creation thresholds, where the cross section for these processes are large.

When the function $\eta(s)$ includes all FSR, from the maximum allowed real radiation to the soft photon cut-off, the correction factor would modify the cross section to account for all, real and virtual, FSR. This is called an inclusive correction. How much of the FSR corrections have been included in the experimental cross section is not always known, however, so one may employ a conservative correction factor of the form

$$C_{fsr} = \left(1 + 0.5\,\eta(s)\frac{\alpha}{\pi}\right) \pm 0.5\,\eta(s)\frac{\alpha}{\pi}.$$

This correction factor spans the range between including and excluding all of the FSR corrections. In some cases, however, it is experimentally known that not all of the real FSR has been accounted for. In other words, experimental cuts can remove those events which are accompanied by FSR of certain types, thus affecting the cross section for that process. We will return to experimental cuts and their effect on the FSR correction later on.

Another source of error which must be considered when calculating the anomalous magnetic moment is that arising from combining data sets. Calculating the anomalous moment below 11 GeV requires the use of experimentally measured cross sections, which means combining a number of experiments measuring various channels at various energies. This combination process aims to minimise the amount of theoretical assumption on the shape and normalisation of the cross section as a function of energy. This means, for instance, avoiding the use of a Breit-Wigner distribution fit.

One way one might consider combining the data would be to calculate the integral for the anomalous moment separately for each experiment, and then taking the weighted average of the results. This has certain associated problems, such as incorrect error evaluation and

the problem of sparsely populated data sets. Alternatively, one might integrate over all data points in a particular channel and use that value as the anomalous moment contribution for, say, the K+K- channel. This has its own difficulties, for instance the weighting of precise data may be reduced by nearby, large error data points, leading to an overall error overestimation. The approach taken is therefore that one should combine the data before integration, for each particular channel.

The first step is to break up the data points in a particular channel into clusters, groupings of data points into energy binnings, assuming that the cross section within a cluster is constant. Recalling the definition of $R(s)$,

$$R(s) = \frac{\sigma^0_{had}(s)}{\sigma_{pt}(s)},$$

one defines the equation

$$R\left(\sqrt{s} = E_i^{(k,m)}\right) = R_i^{(k,m)} \pm \left[\left(dR_i^{(k,m)}\right)^2 + \left(df_k R_i^{(k,m)}\right)^2\right]^{1/2} = R_i^{(k,m)} \pm d\tilde{R}_i^{(k,m)}$$

where $R_i^{(k,m)}$ is the ith $R(s)$ value for experiment k in cluster m. $E_i^{(k,m)}$ is the energy of the data points in this cluster, df_k is the common systematic error of the data points in experiment k (as a percentage), and $dR_i^{(k,m)}$ is the contribution from any other systematic uncertainties. The weighted average for cluster m is then given by

$$R_m = \left[\sum_k \sum_{i=1}^{N(k,m)} \frac{R_i^{(k,m)}}{\left(d\tilde{R}_i^{(k,m)}\right)^2}\right]\left[\sum_k \sum_{i=1}^{N(k,m)} \frac{1}{\left(d\tilde{R}_i^{(k,m)}\right)^2}\right]^{-1}.$$

The energy for each of these clusters is given by the equation

$$E_m = \left[\sum_k \sum_{i=1}^{N(k,m)} \frac{E_i^{(k,m)}}{\left(d\tilde{R}_i^{(k,m)}\right)^2}\right]\left[\sum_k \sum_{i=1}^{N(k,m)} \frac{1}{\left(d\tilde{R}_i^{(k,m)}\right)^2}\right]^{-1}.$$

This estimate of the weighted average R for cluster m is only a starting value, which will be used in a χ^2 minimisation function, to determine the final R_m values. This function is

$$\chi^2(R_m, f_k) = \sum_k^{N_{exp}} \left(\frac{1-f_k}{df_k}\right)^2 + \left\{\sum_{m=1}^{N_{clu}} \sum_{i=1}^{N(k,m)} \left(\frac{R_i^{(k,m)} - f_k R_m}{d\tilde{R}_i^{(k,m)}}\right)^2\right\}_{w/o\ covariance\ matrix}$$
$$+ \left\{\sum_{m=1}^{N_{clu}} \sum_{i=1}^{N(k,m)} \sum_{j=1}^{N(k,n)} \left(R_i^{(k,m)} - f_k R_m\right) C^{-1}(m_i, n_j) \left(R_j^{(k,n)} - f_k R_n\right)\right\}.$$

This function fits the values of R_m and f_k, which are the $R(s)$ value for cluster m and the normalisation factor for the kth experiment. C^{-1} is the inverse of the covariance matrix. Given that some recent experiments quote a covariance matrix for their statistical and systematic errors, the second term on the right takes account of those experiments which do not have a covariance matrix, and the third term those that do. Minimising the above function by changing the parameters R_m and f_k gives the fitted values $\bar{R}_m$ and $\bar{f}_k$.

Once the $\bar{R}_m$ and $\bar{f}_k$ values have been found, one may use the trapezoid rule to calculate the integral over the $R(s)$ values and hence the anomalous moment. Recalling the integral for the hadronic contribution to the anomalous moment of the muon to leading order,

$$a_\mu^{had,LO} = \left(\frac{\alpha m_\mu}{3\pi}\right)^2 \int_{s_{th}}^{\infty} ds\ \frac{R(s)K(s)}{s^2},$$

and changing variables from s, the centre of mass energy squared, to the centre of mass energy E, one finds (ignoring constant prefactors)

$$I = \int_{s_{th}}^{\infty} ds\ \frac{R(s)K(s)}{s^2} = 2\int_{E_a}^{E_b} \frac{dE}{E^2} E\ R(E^2)K(E^2),$$

with an associated error ΔI. Making the definitions that $E_m < E_a < E_{m+1}$ which is less than $E_{n-1} < E_b < E_n$. The integral I can then be evaluated as

$$I = 2\left(\frac{E_{m+1} - E_a}{2E_a}\bar{R}_a K_a + \frac{E_{m+2} - E_a}{2E_{m+1}}\bar{R}_{m+1}K_{m+1}\right) + 2\left(\sum_{l=m+1}^{n-2} \frac{E_{l+1} - E_{l-1}}{2E_l}\bar{R}_l K_l\right)$$
$$+ 2\left(\frac{E_b - E_{n-2}}{2E_{n-1}}\bar{R}_{n-1}K_{n-1} + \frac{E_b - E_{n-1}}{2E_b}\bar{R}_b K_b\right),$$

where $K_l = K(E_l^2)$ and linear interpolation is used to find $\bar{R}_a$ and $\bar{R}_b$. The error ΔI is given by

$$(\Delta I)^2 = \sum_{p=m}^{n}\sum_{q=m}^{n}\frac{\partial I}{\partial \bar{R}_p}\tilde{V}(p,q)\frac{\partial I}{\partial \bar{R}_q} = \sum_{p,q=m}^{n}\left(\frac{E_{p+1}-E_{p-1}}{E_p}K_p\right)\tilde{V}(p,q)\left(\frac{E_{q+1}-E_{q-1}}{E_q}K_q\right),$$

where $\tilde{V}(p,q)$ is the inflated covariance matrix.

Chapter 4

Minimisation of errors in the hadronic K^+K^- channel

The aim of this project is to investigate how much the error on the anomalous magnetic moment could be reduced, beginning with the $e^+e^- \rightarrow \gamma^* \rightarrow K^+K^-$ channel, and time permitting moving to other channels. This is done in two ways. Firstly, researching those experiments which measured the $e^+e^- \rightarrow \gamma^* \rightarrow K^+K^-$ cross section and changing which data sets were included in the anomalous magnetic moment contribution calculation based on systematic error, data energy range, data set size etc, one could investigate how this affected the anomalous magnetic dipole moment K^+K^- contribution and the associated error. Secondly, researching the experimental cuts utilised by each experiment allows one to change the FSR correction value and so to reduce the error.

At a centre of mass energy of $\sqrt{s}$ =10 GeV, the contribution the anomalous magnetic moment from the K^+K^- channel is approximately 3.42 %, making it the third largest contribution after $\pi^+\pi^-$ (78.15%) and $\pi^+\pi^-\pi^0$ (7.22%) (9). The K^+K^- data consists of 13 data from eleven different publications spanning a period of 31 years, from data published in 1977 from the MEA magnetic apparatus at the ADONE experiment, located at the Frascati National Laboratory in Rome (17) (18), to the CMD-2 cryogenic magnetic detector at the VEPP-2M electron-positron collider at the Budker Institute for Nuclear Physics in Novosibirsk, which published $e^+e^- \rightarrow \phi \rightarrow K^+K^-$ cross section measurements in 2008 (19) (20) (21)[3].

The question might be posed: why would one want to remove any of the data sets? Combining low error sets with consistent high error sets should never make the combined error go up and should, if anything, *decrease* the error, if only slightly. The combination, however, of inconsistent sets *is* liable to make the error increase, and so the first part of this project is essentially an investigation into whether or not the sets are consistent with each other, and indeed if removal of data sets would be a wise thing to do at all.

[3] A new data set was released from the Babar experiment in June 2013, but was not included in the data sets used in this thesis due to this recent release date. The source can be found in reference (30)

4.1 Data set selection

In order to investigate which data sets were to be included and which omitted from the calculation of the anomalous moment, one first had to make a table detailing the information within the 13 data publications about how they processed the data[4]. The areas of interest are; the magnitude of the systematic errors associated with the measurements, details of how they accounted for vacuum polarizations in the cross section, in other words whether or not the stated cross section is the measured cross section, and finally the FSR corrections. The details of the publications are shown in the table below.

[4] Note that there are eleven publications but 13 data sets. This is simply a consequence of the fact that the CMD-2 experiment from 2008 and SND experiment from 2001 published two different scans.

Name of publication	Authors	Publication date	Name of Experiment
Measurement of $e^+e^- \rightarrow \phi \rightarrow K^+K^-$ cross section with CMD-2 detector at VEPP-2M Collider	R.R. Akhmetshin et al	1 April 2008	CMD-2 detector, VEPP-2M Collider, Budker Institute for Nuclear Physics, Novosibirsk (19) (20) (21)
Measurement of the $e^+e^- \rightarrow K^+K^-$ cross section in the enrgy range $\sqrt{s}$ =1.05-1.38 GeV with the SND detector at VEPP-2M e^+e^- collider	M.N. Achasov et al	13 November 2007	SND experiment, VEPP-2M Collider, Budker Institute for Nuclear Physics, Novosibirsk (19) (20) (22)
Momentum analysis of Kaon and Pion pairs produced from time-like photons at 1.6 GeV energy	B. Esposito et al	28 March 1977	MEA magnetic apparatus, ADONE experiment, Frascati National Laboratory,Rome (17) (18)
Unable to locate reference	N/A	N/A	BCF detector, ADONE experiment, Frascati National Laboratory,Rome (17) (18)
Study of the reaction $e^+e^- \rightarrow K^+K^-$ in the total energy range 1400-2060 MeV	B. Delcourt et al	19 February 1981	Magnetic detector DM1 (23), Orsay colliding Beam facility DCI (24).
Study of the reaction $e^+e^- \rightarrow K^+K^-$ in the energy range $1350 \leq \sqrt{s} \leq 2400$ MeV	D. Bisello et al	1988	Magnetic detector DM2, Orsay colliding Beam facility DCI (24) (25).
Unable to locate reference	N/A	1983	DM2 Brighton Conference, DM2 experiment, Orsay colliding Beam facility DCI (24) (25).
Measurement of the charged kaon form factor in the energy range 1.0 to 1.4 GeV.	P.M. Ivanov et al	31 August 1981	OLYA detector (26), VEPP-2M Collider, Budker Institute for Nuclear Physics, Novosibirsk (19) (20)
Summary of experiments with the Neutral Detector at the e^+e^- storage ring VEPP-2M	S.I. Dolinsky et al	1991	Neutral Detector (27), VEPP-2M Collider, Budker Institute for Nuclear Physics, Novosibirsk (19) (20)
Measurement of the ϕ meson parameters with the CMD-2 detector at the VEPP-2M collider	R.R. Akhmetshin et al	1995	CMD-2 detector, VEPP-2M Collider, Budker Institute for Nuclear Physics, Novosibirsk (19) (20) (21)
Measurements of the parameters of the $\phi(1020)$ resonance through studies of the processes $e^+e^- \rightarrow K^+K^-$, K_SK_L and $\pi^+\pi^-\pi^0$	M.N. Achasov et al	6 March 2001	SND experiment, VEPP-2M Collider, Budker Institute for Nuclear Physics, Novosibirsk (19) (20) (22)

Table 1: Publications of the data used in the K+K- channel.

As mentioned, two of the publications, those from the BCF detector at the ADONE experiment and the DM2 Brighton conference paper, were not sourced. The publications

listed above were then searched for information on systematic errors and FSR corrections, while the vacuum polarization correction types were found in reference (16). A table of this information was then compiled and is shown below.

Experiment Name (Year of publication)	Systematic Error	VP Correction Type*	FSR Correction†
CMD-2 (2008)	"The systematic error of the cross section is estimated to be 2.2%". Extensive discussion of systematic error sources. ISR included; determined to a 0.5% accuracy. Quoted code value : 2%	Not present, further references perhaps needed.	ISR corrected for in accordance with Kuraev and Fadin (1985), but no mention of FSR.
SND (2007)	Systematic errors quoted separately for the cross section corresponding to each energy.	The born cross section is quoted, suggesting that VP corrections have been applied. The normalisation, either muon pair production or Bhabha scattering, is not mentioned.	No explicit mention of FSR, only referring to a radiative correction factor. Kuraev and Fadin (1985) paper cited.
MEA (1977)	Does not appear to be present in paper, further references perhaps needed. Quoted code value : 10%	D (Bhabha scattering normalisation; electron and muon vacuum polarisation contributions included)	Not present, further references perhaps needed.
BCF ADONE	Unable to locate reference Quoted code value : 10%	Unable to locate reference	Unable to locate reference
DM1-DCI (1981)	"The overall systematic error is estimated to be at most 6%; ±2% on the $\pi^+\pi^-$ contamination, ±1% on the tracking efficiency and ±3% on the radiative corrections". Quoted code value : 6%	D (Bhabha scattering normalisation; electron and muon vacuum polarisation contributions included)	Not present, see systematic errors
DM2-DCI (1988)	No mention of systematic errors within reference; assumption of maximum value must be inferred and applied. Quoted code value : 6.5%	B(C_{VP} = 1)	No mention whatever of radiative corrections, FSR or otherwise. Other reference perhaps needed.
DM2 Brighton Conference (1983)	Unable to locate reference Quoted code value : 10%	Unable to locate reference	Unable to locate reference
OLYA (1981)	"The most precise measurement of the cross section (10% statistical and 10% systematic uncertainties) was performed with the OLYA detector at the VEPP-2M collider" SND (2007) Quoted code value : 10%	D (Bhabha scattering normalisation; electron and muon vacuum polarisation contributions included)	No mention whatever of radiative corrections, FSR or otherwise. Other reference perhaps needed.

Neutral Detector (1991)	"The systematic error of R(s) is estimated to be about 10%". Quoted code value : 10%	D (Bhabha scattering normalisation; electron and muon vacuum polarisation contributions included)	Not Present
CMD-2 (1995)	"When the number of hadronic events is normalised to the number of collinear events the systematic uncertainties of the reconstruction efficiency cancel to the level of 2% included in the systematic uncertainty of each point". Quoted code value : 4.1%	A (Effects from s-channel photon vacuum polarisation corrections)	"For leptonic channels the radiation of both initial and final state particles was taken into account".
SND (2001)	Systematic errors for all $e^+e^- \rightarrow K^+K^-$ cross sections are quoted in table as 7.1%. Quoted code value : 7.1%	A (Effects from s-channel photon vacuum polarisation corrections)	Not Present

Table 2: Literature search table detailing mentions of systematic errors, VP correction types and FSR corrections for the K+K- channel data

* See K. Hagiwara et al, physical review D, 2004, for VP correctional procedure types. Specific correction values are also quoted in the reference for all publications pre-2004.

†Here, green font indicates a thorough discussion of the error or correction in question, blue indicates partial information, and red indicates no mention whatsoever.

It is assumed above that Initial State Radiation (ISR) corrections have already been applied by each experiment. In the rare cases in which ISR is not accounted for one has to do de-convolution with respect to ISR. This is not relevant to the K+K- channel, because this procedure has already been applied. A consideration which has not been taken into account by the preceding table is the energy range which is covered by each data set. This must also be taken into account; otherwise large gaps in the integration range will be fitted via the trapezoidal rule and incur a large error. Therefore, one must attempt to chose a group of sets by judiciously balancing the criteria of having reasonably low systematic errors, being fairly modern (and so more likely to include some information on FSR corrections) and have a large number of points covering a wide energy range. After studying this table and the following graphs of energy coverage, it was decided to calculate the anomalous magnetic moment and the associated error for three custom sets; a set which includes all eleven data sets, a set which only includes those data sets with low systematic errors, and a 'modern' set. Here, low systematic errors are defined to be errors of less than ten percent, and modern sets are those published in or after 1990. The table displaying these sets is shown below.

Full Set	Low systematic errors set	Modern Set
CMD-2 Scan 1 (2008) CMD-2 Scan 2 (2008) SND (2007) MEA-ADONE (1977) BCF-ADONE (1986) DM1-DCI (1981) DM2-DCI (1987) DM2 (1983) OLYA (1981) ND (1991) CMD-2 (1995) SND Scan 1 (2001) SND Scan 2 (2001)	CMD-2 Scan 1 (2008) CMD-2 Scan 2 (2008) SND (2007) DM1-DCI (1981) DM2-DCI (1987) CMD-2 (1995) SND Scan 1 (2001) SND Scan 2 (2001)	CMD-2 Scan 1 (2008) CMD-2 Scan 2 (2008) SND (2007) ND (1991) CMD-2 (1995) SND Scan 1 (2001) SND Scan 2 (2001)

Table 3: Details of data sets chosen to make up the Full, Low Systematic and Modern sets.

The first step in checking these data sets was to recalculate the anomalous magnetic moment and associated error using the full set, the 'modern' set, and the low systematics set, comparing the error and chi squared values for each. These results are displayed below.

Data Set Selection Criteria	Anomalous magnetic moment ($\times 10^{-10}$)	Anomalous magnetic moment (with linear fit) ($\times 10^{-10}$)	Chi squared per degree of freedom
All 13 sets	22.1631 ± 0.4628	21.5736 ± 0.1653	1.8652
Only sets with < 10% systematic error (4,5,8,9,10†)	22.3650 ± 0.3686	22.1304 ± 0.1177	1.7207
'Modern' set (1990s and onwards) (4,5,6,7,8,9†)	21. 4084 ± 0.3766	21.0719 ± 0.1124	2.0076

Table 4: Results of the use of the various custom sets to calculate the anomalous magnetic moment, the error and the chi squared value.

† Those experiments which have been removed from the calculation

1 = CMD-2 Scan 1 (2008) 2 = CMD-2 Scan 2 (2008)
3 = SND (2007) 4 = MEA-ADONE (1977)
5 = BCF-ADONE (1986) 6 = DM1-DCI (1981)
7 = DM2-DCI (1987) 8 = DM2 (1983)
9 = OLYA (1981) 10 = CMD (1991)
11 = CMD-2 (1995) 12 = SND Scan 1 (2001)
13 = SND Scan 2 (2001)

The errors associated with both the reduced sets are smaller than that of the full set, yet the modern set does not fit the distribution as well as the full set does. The next step was to check the energy coverage of the sets, as shown below.

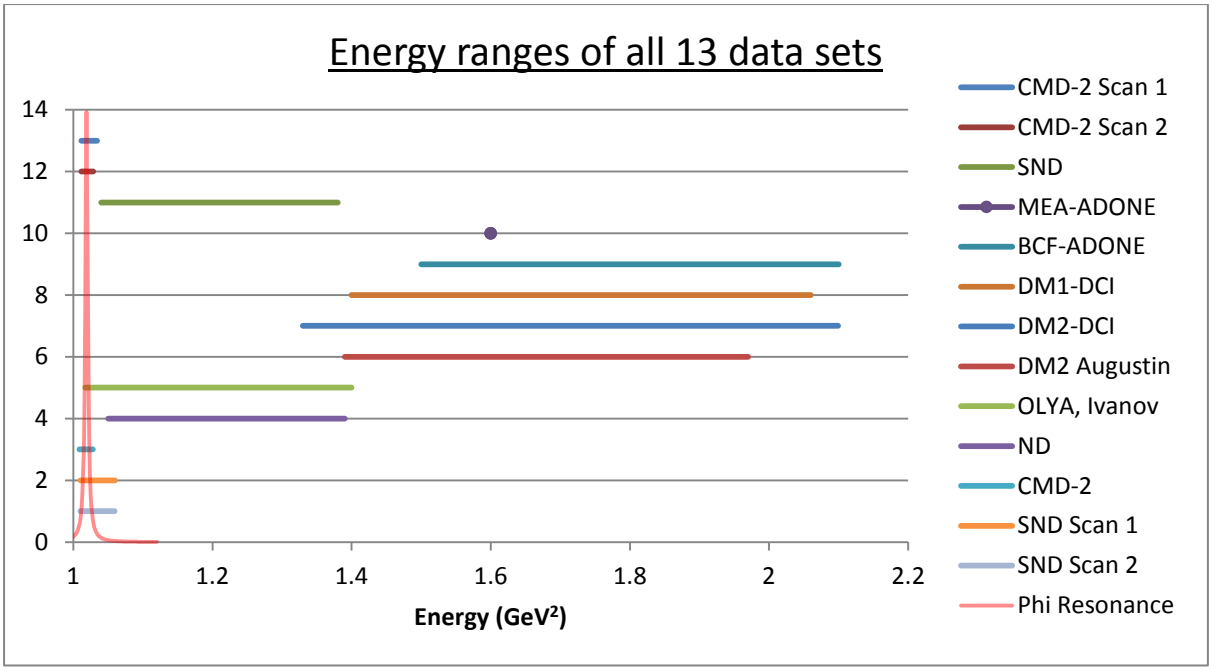

Figure 5: Energy range of the full data set.

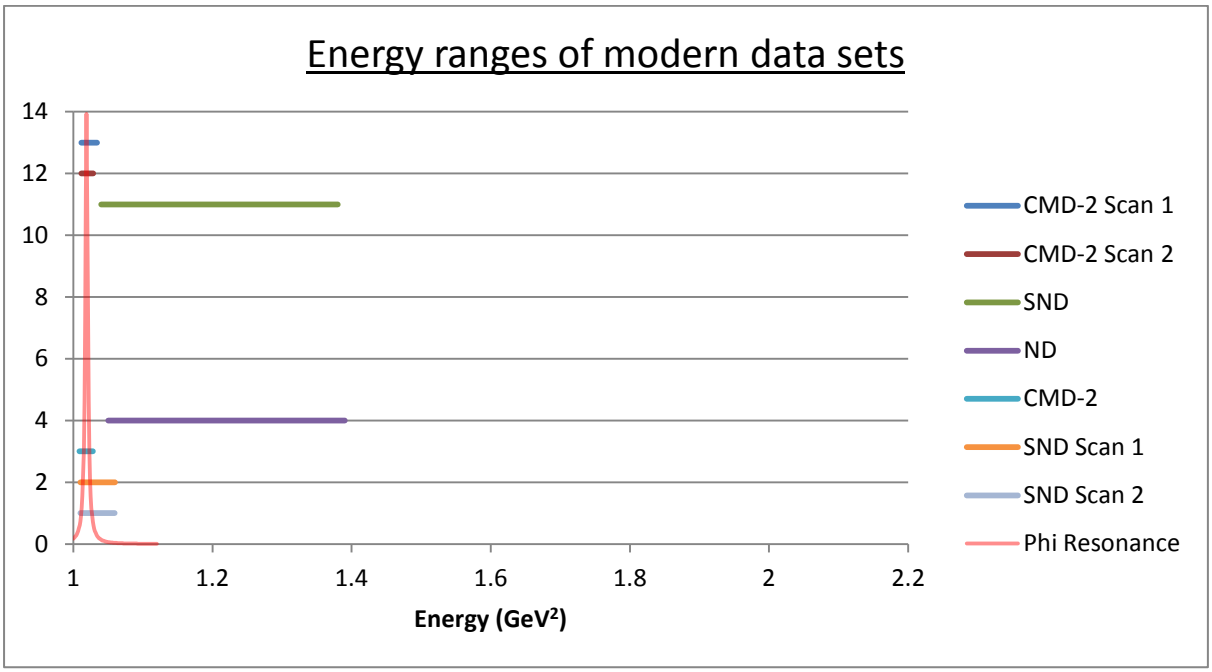

Figure 6: Energy range of the modern data set

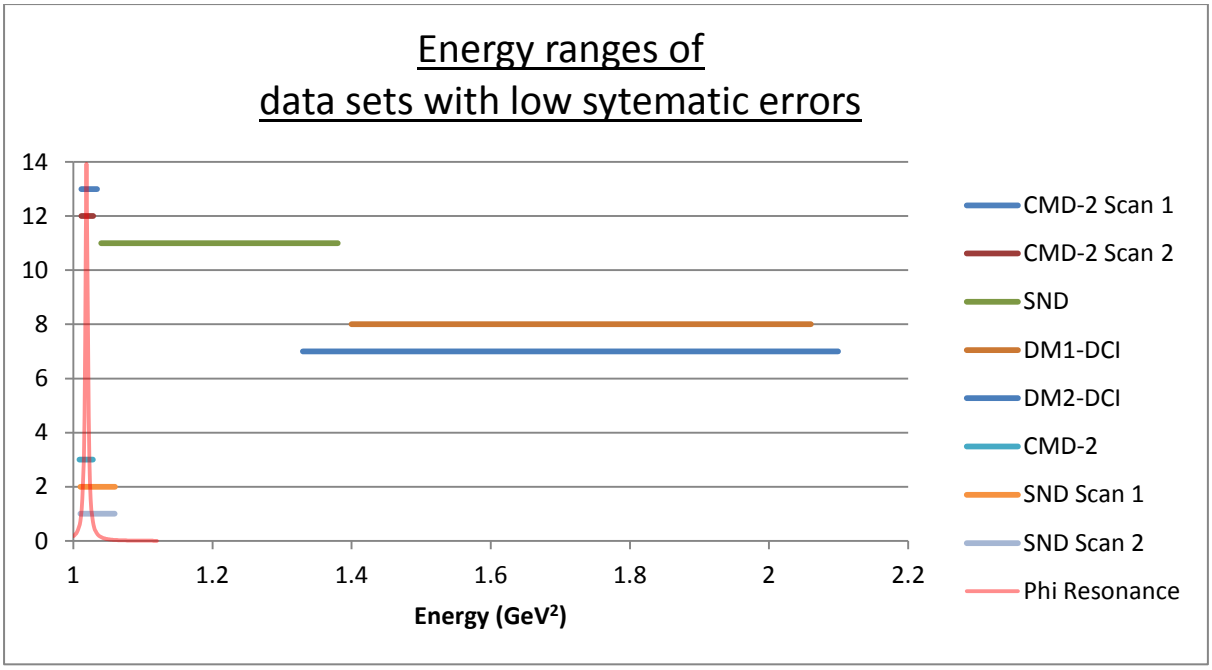

Figure 7: Energy range of the low systematic error data set

In all three of the above graphs, the name of experiment and its representation on the graph are in the same vertical order. It is clear that, whilst having plenty of data sets on the phi peak, the modern data set grouping fails to cover the whole range of the energies over which the cross section is measured. The low systematic set, however, has the same sets as the modern set on the phi resonance but also includes sets which cover the mid and high energy range too. The K^+K^- cross section is heavily suppressed far away from the phi peak, so it is worthwhile checking the low, low-mid and full energy range (defined below) behaviour of the errors. This is done by changing the upper integration limit on the equation which calculates the anomalous moment. These calculations are shown below.

Full energy range integration	**Anomalous magnetic moment**	**Chi squared per degree of freedom**
All Data Sets	22.1631 ± 0.4628	1.8652
Low Systematic errors	22.3650 ± 0.3686	1.7207
Modern Sets	Data set does not extend over full energy range, and hence value would be identical to low-mid energy range integration (see lowermost table).	-

Table 5: Comparison between custom sets over full energy range.

Low energy range integration (1.01- 1.06 GeV^2)	**Anomalous magnetic moment**	**Chi squared per degree of freedom**
All Data Sets	17.8066 ± 0.4228	1.8652
Low Systematic errors	17.8765 ± 0.3354	1.7207
Modern Sets	17.8994 ± 0.3388	2.0076

Table 6: Comparison between custom sets over low energy range.

Low-mid energy range integration (1.01- 1.4 GeV^2)	**Anomalous magnetic moment**	**Chi squared per degree of freedom**
All Data Sets	21.2733 ± 0.4581	1.8652
Low Systematic errors	21.4307 ± 0.3614	1.7207
Modern Sets	21.4084 ± 0.3766	2.0076

Table 7: Comparison between custom sets over low-mid energy range.

As the above data shows, the error increases as the higher energy data sets are included, for all three of the set groupings. The low systematic group is, however, consistently the lowest, has the best chi squared degree of freedom and covers the full energy range. This exercise shows that indeed the error does decrease when certain sets are judiciously removed, with an approximately 20% decrease in the error when using the low systematics grouping.

4.2 FSR correction factor

The cross section value depends on the amount of phase space which has been included in its measurement. If an experiment makes cuts based on acolinearity of the two kaons, then this is effectively an FSR phase space cut. In other words, discarding those events which are beyond the acolinearity maximum threshold means that those events which were acolinear because of sufficiently hard FSR will be discarded, and hence the contribution from this phase space range towards the cross section value will be lost.

In order to correct the cross section value to include all of the final state radiation, one must apply a correction factor to the cross section, C_{fsr} . By including all final state radiation one means including all virtual radiation and the full range of possible real radiation, from the maximum energy a radiated photon could have whilst leaving enough energy for a pair of kaons, down to a minimum energy cut off. This correction factor (17) takes the form

$$C_{fsr} = 1 + \eta(s)\frac{\alpha}{\pi},$$

where α is the fine structure constant and s is the centre of mass energy squared. The correction factor is applied to the theoretical born cross section (29) in order to calculate the FSR corrected cross section

$$\sigma_{fin} = \left(1 + \eta(s)\frac{\alpha}{\pi}\right)\sigma_0 \,.$$

$\eta(s)$ is in turn defined by the equation

$$\eta(s) \equiv \frac{\pi}{\alpha}\left[\delta_{fin}(\Lambda) + \int_{4m_K^2}^{s-2\sqrt{s}\Lambda} ds'\, \rho_{fin}(s,s')\right].$$

The first term on the right hand side of the above equation corrects for virtual FSR and soft real radiation contributions and the second term sums over all possible detectable real radiation. In order to calculate $\eta(s)$, one must therefore integrate the function $\rho_{fin}(s,s')$ over s', s' being the invariant mass squared of the kaon pair, from the lower limit of the minimum energy required to create a pair of kaons up to the maximum energy the kaon system could have whilst also emitting some real radiation. This involves the use of a regulator, Λ , which encodes the minimum energy an emitted photon could carry away from the kaon system.

In order to calculate the FSR corrected cross section from the born cross section, one must include all possible, real and virtual, corrections. This involves setting the non-physical regulator to zero at the end of the calculation. Such a cross section is known as *inclusive.* In our case, however, we are not correcting a theoretical born cross section but a measured one, with all virtual and soft real corrections necessarily included and the real correction dependant on an experimentally dictated regulator, $\widetilde{\Lambda}$. This changes the form of the above equation to

$$I(s) \equiv \frac{\pi}{\alpha}\left[\int_{4m_K^2}^{s-2\sqrt{s}\widetilde{\Lambda}} ds'\,\rho_{fin}(s,s')\right].$$

It is this correction we will use to correct the experimental cross sections (29). $\rho_{fin}(s,s')$ has the form

$$\rho_{fin}(s,s') = \frac{1}{s}\left[\tilde{\delta}_{fin}^{H}(s,s') + \frac{B_k(s,s')}{1-z}\right]$$

$$= \frac{1}{s}\left[\frac{2\alpha}{\pi}(1-z)\frac{\beta(s')}{\beta^3(s)} + \frac{1}{1-z}\,\frac{2\alpha}{\pi}\frac{s'\beta(s')}{s\beta(s)} \times \left[\frac{1+\beta^2(s')}{2\beta(s')}\log\left(\frac{1+\beta(s')}{1-\beta(s')}\right) - 1\right]\right],$$

where

$$\beta(x) = \sqrt{1-\frac{4m_K^2}{x}}\ , \qquad z = \frac{s'}{s}.$$

This then reduces to solving the integrals

$$\int_{4m_K^2}^{s-2\sqrt{s}\widetilde{\Lambda}} ds'\,\rho_{fin}(s,s')$$

$$= \frac{2\alpha}{\pi s}\left[\int_{4m_K^2}^{s-2\sqrt{s}\widetilde{\Lambda}} ds'\frac{\beta(s')}{\beta(s)^3} - \frac{1}{s}\int_{4m_K^2}^{s-2\sqrt{s}\widetilde{\Lambda}} ds's'\frac{\beta(s')}{\beta(s)^3}\right.$$

$$\left. + \int_{4m_K^2}^{s-2\sqrt{s}\widetilde{\Lambda}} ds'\frac{s'}{s-s'}\frac{\beta(s')}{\beta(s)}\left\{\frac{1+\beta(s')^2}{2\beta(s')}\log\left(\frac{1+\beta(s')}{1-\beta(s')}\right) - 1\right\}\right].$$

The main part of this project was therefore to calculate the above integral with an experimentally dependant regulator, and use the resulting correction factor to revaluate the cross section value. In order to solve these integrals, it is helpful to change the integration

variable from s' to $\beta(s')$. Adopting this strategy and integrating term by term, one proceeds as follows.

Term 1

$$\int_{4m_K^2}^{s-2\sqrt{s}\widetilde{\Lambda}} ds' \frac{\beta(s')}{\beta(s)^3} = \frac{1}{\beta(s)^3}\int_{4m_K^2}^{s-2\sqrt{s}\widetilde{\Lambda}} ds'\beta(s')$$

Changing the variable s' to $\beta(s')$ transforms the above equation to

$$\frac{1}{\beta(s)^3}\int_{4m_K^2}^{s-2\sqrt{s}\widetilde{\Lambda}} ds'\beta(s') = \frac{8m_K^2}{\beta(s)^3}\int_0^{\chi} d\beta(s')\frac{\beta^2(s')}{(1-\beta^2(s'))^2}\,.$$

The new upper limit as required by the new variable is defined as

$$\chi \equiv \sqrt{1-\frac{4m_K^2}{s-2\sqrt{s}\widetilde{\Lambda}}},$$

where the lower limit is zero. The solution of an integral of this type is given by

$$\int dx\,\frac{x^2}{(1-x^2)^2} = \frac{1}{4}\left(-\frac{2x}{x^2-1} + \log(1-x) - \log(x+1)\right)$$

$$= \frac{1}{4}\left(-\frac{2x}{x^2-1} + \log\left(\frac{1-x}{x+1}\right)\right).$$

The result of integrating term 1 is therefore

$$\frac{1}{\beta(s)^3}\int_{4m_K^2}^{s-2\sqrt{s}\widetilde{\Lambda}} ds'\beta(s') = \frac{2m_K^2}{\beta(s)^3}\left(\frac{2\chi(s-2\sqrt{s}\widetilde{\Lambda})}{4m_K^2} + \log\left(\frac{1-\chi}{1+\chi}\right)\right).$$

Term 2

$$-\frac{1}{s}\int_{4m_K^2}^{s-2\sqrt{s}\widetilde{\Lambda}} ds's'\frac{\beta(s')}{\beta(s)^3} = -\frac{1}{s\beta(s)^3}\int_{4m_K^2}^{s-2\sqrt{s}\widetilde{\Lambda}} ds's'\beta(s')$$

$$= -\frac{32m_K^4}{s\beta(s)^3}\int_0^{\chi} d\beta(s')\frac{\beta^2(s')}{(1-\beta^2(s'))^3}$$

The general solution to the above integral is

$$\int \frac{x^2}{(1-x^2)^3} = \frac{1}{16}\left(\frac{2(x^3+x)}{(x^2-1)^2} - \log(-x-1) + \log(x-1)\right).$$

Notice that, for 0 < x < 1, both of the log terms in this solution are complex. Combining these two terms together, as was done for term 1, acts to solve this problem. The solution to the term 2 integral is therefore

$$-\frac{1}{s}\int_{4m_K^2}^{s-2\sqrt{s}\widetilde{\Lambda}} ds' s' \frac{\beta(s')}{\beta(s)^3} = -\frac{2m_k^4}{s\beta(s)^3}\left[\frac{2(\chi^3+\chi)}{(\chi^2-1)^2} + \log\left(\frac{1-\chi}{1+\chi}\right)\right].$$

Term 3

The third term must be split up further into smaller, more manageable pieces. This procedure is shown below.

$$\int_{4m_K^2}^{s-2\sqrt{s}\widetilde{\Lambda}} ds' \frac{s'}{s-s'}\frac{\beta(s')}{\beta(s)}\left\{\frac{1+\beta(s')^2}{2\beta(s')}\log\left(\frac{1+\ \beta(s')}{1-\ \beta(s')}\right) - 1\right\}$$

$$= \frac{1}{\beta(s)}\int_{4m_K^2}^{s-2\sqrt{s}\widetilde{\Lambda}} ds' \frac{s'}{s-s'}\beta(s')\left\{\frac{1+\beta(s')^2}{2\beta(s')}\log\left(\frac{1+\ \beta(s')}{1-\ \beta(s')}\right) - 1\right\}$$

$$= \frac{1}{\beta(s)}\int_{4m_K^2}^{s-2\sqrt{s}\widetilde{\Lambda}} ds' \frac{s'}{s-s'}\beta(s')\left\{\frac{1+\beta(s')^2}{2\beta(s')}\log\left(\frac{1+\ \beta(s')}{1-\ \beta(s')}\right)\right\} - \frac{1}{\beta(s)}\int_{4m_K^2}^{s-2\sqrt{s}\widetilde{\Lambda}} ds' \frac{s'}{s-s'}\beta(s')$$

Exploiting the fact that

$$\frac{s'}{s-s'} = -1 + \frac{s}{s-s'}$$

allows one to split this integral up further to give

$$\int_{4m_K^2}^{s-2\sqrt{s}\widetilde{\Lambda}} ds' \frac{s'}{s-s'}\frac{\beta(s')}{\beta(s)}\left\{\frac{1+\beta(s')^2}{2\beta(s')}\log\left(\frac{1+\beta(s')}{1-\beta(s')}\right)-1\right\}$$

$$= \frac{1}{\beta(s)}\left[-\frac{1}{2}\int_{4m_K^2}^{s-2\sqrt{s}\widetilde{\Lambda}} ds' \log\left(\frac{1+\beta(s')}{1-\beta(s')}\right) - \frac{1}{2}\int_{4m_K^2}^{s-2\sqrt{s}\widetilde{\Lambda}} ds' \,\beta(s')^2 \log\left(\frac{1+\beta(s')}{1-\beta(s')}\right)\right.$$

$$+ \quad \frac{s}{2}\int_{4m_K^2}^{s-2\sqrt{s}\widetilde{\Lambda}} ds' \frac{1}{s-s'}\log\left(\frac{1+\beta(s')}{1-\beta(s')}\right)$$

$$+ \quad \frac{s}{2}\int_{4m_K^2}^{s-2\sqrt{s}\widetilde{\Lambda}} ds' \frac{1}{s-s'}\beta(s')^2 \log\left(\frac{1+\beta(s')}{1-\beta(s')}\right) + \int_{4m_K^2}^{s-2\sqrt{s}\widetilde{\Lambda}} ds' \,\beta(s')$$

$$\left. - s\int_{4m_K^2}^{s-2\sqrt{s}\widetilde{\Lambda}} ds' \frac{1}{s-s'}\beta(s')\right].$$

We will henceforth for convenience refer to the above six terms on the right hand side as terms A through F.

Term A

Using the substitutions

$$u = \frac{1+\beta(s')}{1-\beta(s')} \quad \text{and} \quad \frac{du}{dx} = \frac{2}{1-\beta(s')^2} \ ,$$

Term A becomes

$$-\frac{1}{2}\int_{4m_K^2}^{s-2\sqrt{s}\widetilde{\Lambda}} ds' \log\left(\frac{1+\beta(s')}{1-\beta(s')}\right) = \ -4m_K^2\left[\frac{1}{8}\int\left(1-\frac{1}{u}\right)\log(u)\,du\right].$$

Integrating this and reverting to the original variables results in the solution

$$-\frac{1}{2}\int_{4m_K^2}^{s-2\sqrt{s}\widetilde{\Lambda}} ds' \log\left(\frac{1+\beta(s')}{1-\beta(s')}\right) = \ -m_K^2\left[\left(\frac{1+\chi^2}{1-\chi^2}\right)\log\left(\frac{1+\chi}{1-\chi}\right) - \frac{2\chi}{1-\chi^2}\right].$$

Term B

$$-\frac{1}{2}\int_{4m_K^2}^{s-2\sqrt{s}\tilde{\Lambda}} ds'\,\beta(s')^2\log\left(\frac{1+\beta(s')}{1-\beta(s')}\right)$$
$$= -4m_K^2\left[\int_0^{\chi} d\beta(s')\frac{\beta(s')^3}{\left(1-\beta^2(s')\right)^2}\log\left(1+\beta(s')\right)\right.$$
$$\left.-\int_0^{\chi} d\beta(s')\frac{\beta(s')^3}{\left(1-\beta^2(s')\right)^2}\log\left(1-\beta(s')\right)\right]$$

The general solutions to the above integrals are

$$\int\frac{x^3\log(1+x)}{(1-\mathrm{x}^2)^2}$$
$$=\frac{1}{4}\left(2\,\mathrm{Li}_2\left(\frac{\mathrm{x}+1}{2}\right)+2\log\left(\frac{1-\mathrm{x}}{2}\right)\log\left(\mathrm{x}+1\right)+\log^2(x+1)-\frac{\log(x+1)}{x-1}\right.$$
$$\left.-\frac{1}{2}\log(x+1)+\frac{1}{2}\log(1-x)+\frac{\log(x+1)+1}{x+1}\right)$$

and

$$\int\frac{x^3\log(1-x)}{(1-\mathrm{x}^2)^2}$$
$$=\frac{1}{4}\left(2\,\mathrm{Li}_2\left(\frac{1-\mathrm{x}}{2}\right)+2\log\left(\frac{\mathrm{x}+1}{2}\right)\log(1-\mathrm{x})-\frac{2\log(1-x)}{x^2-1}+\frac{1}{1-x}\right.$$
$$\left.+\log^2(1-x)-\frac{1}{2}\log(x-1)+\frac{1}{2}\log(1+x)\right).$$

Inserting these into term B and putting in the limits gives

$$-\frac{1}{2}\int_{4m_K^2}^{s-2\sqrt{s}\tilde{\Lambda}} ds'\,\beta(s')^2\log\left(\frac{1+\beta(s')}{1-\beta(s')}\right)$$
$$= -m_K^2\left[\left(2\mathrm{Li}_2\left(\frac{\chi+1}{2}\right)+2\log\left(\frac{1-\chi}{2}\right)\log(\chi+1)+\log^2(\chi+1)-\frac{\log(\chi+1)}{\chi-1}\right.\right.$$
$$-\frac{1}{2}\log(1+\chi)+\frac{1}{2}\log(1-\chi)+\frac{\log(\chi+1)+1}{\chi+1}-2\mathrm{Li}_2\left(\frac{1-\chi}{2}\right)$$
$$-\ 2\log\left(\frac{\chi+1}{2}\right)\log(1-\chi)+\frac{2\log(1-\chi)}{\chi^2-1}-\frac{1}{1-\chi}-\log^2(1-\chi)+\frac{1}{2}\log(\chi-1)$$
$$\left.\left.-\frac{1}{2}\log(1+\chi)\right)-\left(\frac{1}{2}\log\left(-1\right)\right)\right].$$

The term arising from the lower limit is the logarithm of a negative number and so complex. This term, and the other term with a negative logarithmic argument, can be combined to make all of the terms real.

$$-\frac{1}{2}\int_{4m_K^2}^{s-2\sqrt{s}\widetilde{\Lambda}} ds'\,\beta(s')^2 \log\left(\frac{1+\beta(s')}{1-\beta(s')}\right)$$

$$= -m_K^2\left(2\mathrm{Li}_2\left(\frac{\chi+1}{2}\right) - 2\mathrm{Li}_2\left(\frac{1-\chi}{2}\right) + 2\log\left(\frac{1-\chi}{2}\right)\log(\chi+1)\right.$$

$$-\ 2\log\left(\frac{\chi+1}{2}\right)\log(1-\chi)\ + \log^2(\chi+1) - \log^2(1-\chi) + \log\left(\frac{1-\chi}{1+\chi}\right)$$

$$\left. + \frac{2\log(1-\chi)}{\chi^2-1} - \frac{2\log(\chi+1)}{\chi^2-1} + \frac{\chi^2}{\chi^2-1}\right)$$

$$= -m_K^2\left(2\mathrm{Li}_2\left(\frac{\chi+1}{2}\right) - 2\mathrm{Li}_2\left(\frac{1-\chi}{2}\right) + 2\log\left(\frac{1-\chi}{2}\right)\log(\chi+1) - \ 2\log\left(\frac{\chi+1}{2}\right)\log(1-\chi)\right.$$

$$\left. + \log^2(\chi+1) - \log^2(1-\chi) + \log\left(\frac{1-\chi}{1+\chi}\right) + \frac{2}{\chi^2-1}\log\left(\frac{1-\chi}{\chi+1}\right) + \frac{\chi^2}{\chi^2-1}\right)$$

Term C

$$\frac{s}{2}\int_{4m_K^2}^{s-2\sqrt{s}\widetilde{\Lambda}} ds'\,\frac{1}{s-s'}\log\left(\frac{1+\beta(s')}{1-\beta(s')}\right)$$

$$= \frac{s}{2}\int_{4m_K^2}^{s-2\sqrt{s}\widetilde{\Lambda}} ds'\,\frac{1}{s-s'}\log\big(1+\beta(s')\big) - \frac{s}{2}\int_{4m_K^2}^{s-2\sqrt{s}\widetilde{\Lambda}} ds'\,\frac{1}{s-s'}\log\big(1-\beta(s')\big)$$

Terms C and D both contain a component which has an $s - s'$ term in the denominator. Using the identity

$$\frac{1}{s-s'} = \frac{1-\ \beta(s')}{s(1-\beta(s')^2) - 4m_K^2},$$

one may rewrite term C as

$$\frac{s}{2}\int_{4m_K^2}^{s-2\sqrt{s}\tilde{\Lambda}} ds' \frac{1}{s-s'}\log\left(\frac{1+\beta(s')}{1-\beta(s')}\right)$$
$$= 4m_K^2 s\left[\int_0^{\chi} d\beta(s')\frac{\beta(s')}{1-\beta^2(s')}\frac{1}{\left(s\left(1-\beta^2(s')\right)-4m_K^2\right)}\log\left(1+\beta(s')\right)\right.$$
$$\left.-\int_0^{\chi} d\beta(s')\frac{\beta(s')}{1-\beta^2(s')}\frac{1}{\left(s\left(1-\beta^2(s')\right)-4m_K^2\right)}\log\left(1-\beta(s')\right)\right].$$

To proceed further, it is required to break these terms up via partial fractions. For the first term, we will separate those terms which are to be partial fractioned from those which are not,

$$\int_0^{\chi} d\beta(s')\frac{\beta(s')}{1-\beta^2(s')}\frac{1}{\left(s\left(1-\beta^2(s')\right)-4m_K^2\right)}\log\left(1+\beta(s')\right)$$
$$= \int_0^{\chi} d\beta(s')\log\left(1+\beta(s')\right)\left(\frac{\beta(s')}{1-\beta^2(s')}\frac{1}{\left(s\left(1-\beta^2(s')\right)-4m_K^2\right)}\right),$$

where the term which is in brackets is the part which is to be partial fractioned. The general form of this partial fraction is

$$\frac{x}{(1-x^2)(s(1-x^2)-4m_K^2)} = -\frac{sx}{4m_K^2(4m_K^2+sx^2-s)}+\frac{1}{8m_K^2(x-1)}+\frac{1}{8m_K^2(x+1)}.$$

Doing the same for the other term,

$$\int_0^{\chi} d\beta(s')\frac{\beta(s')}{1-\beta^2(s')}\frac{1}{\left(s\left(1-\beta^2(s')\right)-4m_K^2\right)}\log\left(1-\beta(s')\right)$$
$$= \int_0^{\chi} d\beta(s')\log\left(1-\beta(s')\right)\left(\frac{\beta(s')}{1-\beta^2(s')}\frac{1}{\left(s\left(1-\beta^2(s')\right)-4m_K^2\right)}\right),$$

shows that the term which is to be partial fractioned is identical and so obviously gives exactly the same result. Using this method splits term C up into six terms,

$$\frac{s}{2}\int_{4m_K^2}^{s-2\sqrt{s}\tilde{\Lambda}} ds' \frac{1}{s-s'}\log\left(\frac{1+\beta(s')}{1-\beta(s')}\right)$$

$$= s\left[-s\int_0^{\chi} d\beta(s') \frac{\beta(s')\log\left(1+\beta(s')\right)}{s\beta(s')^2-(s-4m_K^2)} + \frac{1}{2}\int_0^{\chi} d\beta(s') \frac{\log\left(1+\beta(s')\right)}{\beta(s')-1}\right.$$

$$+\frac{1}{2}\int_0^{\chi} d\beta(s') \frac{\log\left(1+\beta(s')\right)}{\beta(s')+1} + s\int_0^{\chi} d\beta(s') \frac{\beta(s')\log\left(1-\beta(s')\right)}{s\beta(s')^2-(s-4m_K^2)}$$

$$\left.-\frac{1}{2}\int_0^{\chi} d\beta(s') \frac{\log\left(1-\beta(s')\right)}{\beta(s')-1} - \frac{1}{2}\int_0^{\chi} d\beta(s') \frac{\log\left(1-\beta(s')\right)}{\beta(s')+1}\right].$$

Labelling each term with roman numerals one to six and integrating term by term proceeds as follows.

I

$$\int_0^{\chi} d\beta(s') \frac{\beta(s')\log\left(1+\beta(s')\right)}{s\beta(s')^2-(s-4m_K^2)}$$

$$= \frac{1}{2s}\left(\mathrm{Li}_2\left(\frac{\chi+1}{1-\beta(s)}\right) + \mathrm{Li}_2\left(\frac{\chi+1}{1+\beta(s)}\right) + \log(\chi+1)\log\left(1-\frac{\chi+1}{1-\beta(s)}\right) + \log(\chi\right.$$

$$\left.+1)\log\left(1-\frac{\chi+1}{1+\beta(s)}\right)\right)$$

I I

$$\int_0^{\chi} d\beta(s') \frac{\log\left(1+\beta(s')\right)}{\beta(s')-1} = \mathrm{Li}_2\left(\frac{(\chi+1)}{2}\right) + \log\left(\frac{1-\chi}{2}\right)\ln(\chi+1)$$

I I I

$$\int_0^{\chi} d\beta(s') \frac{\log\left(1+\beta(s')\right)}{\beta(s')+1} = \frac{1}{2}\log^2(\chi+1)$$

IV

$$\int_0^{\chi} d\beta(s') \frac{\beta(s')\log\left(1-\beta(s')\right)}{s\beta(s')^2-(s-4m_K^2)} =$$

$$= \frac{1}{2s}\left(\mathrm{Li}_2\left(-\frac{\chi-1}{1-\beta(s)}\right)+\mathrm{Li}_2\left(-\frac{\chi-1}{1+\beta(s)}\right)+\log(1-\chi)\log\left(\frac{\chi-1}{1-\beta(s)}+1\right)\right.$$

$$\left.+\log(1-\chi)\log\left(\frac{\chi+\beta(s)}{1+\beta(s)}\right)\right)$$

V

$$\int_0^{\chi} d\beta(s') \frac{\log\left(1-\beta(s')\right)}{\beta(s')-1} = \frac{1}{2}\log^2(1-\chi)$$

VI

$$\int_0^{\chi} d\beta(s') \frac{\log\left(1-\beta(s')\right)}{\beta(s')+1} = \mathrm{Li}_2\left(\frac{(1-\chi)}{2}\right)+\log\left(\frac{\chi+1}{2}\right)\ln(1-\chi)$$

The general integrals have been neglected in order to shorten an already lengthy statement of the calculations. Inserting the results of integrating terms one through six results in the total term C integral

$$\frac{s}{2}\int_{4m_K^2}^{s-2\sqrt{s}\tilde{\Lambda}} ds' \frac{1}{s-s'}\log\left(\frac{1+\beta(s')}{1-\beta(s')}\right)$$

$$= s\left[-\frac{1}{2}\left(\mathrm{Li}_2\left(\frac{\chi+1}{1-\beta(s)}\right)+\mathrm{Li}_2\left(\frac{\chi+1}{1+\beta(s)}\right)+\log(\chi+1)\log\left(-\frac{\chi+\beta(s)}{1-\beta(s)}\right)\right.\right.$$

$$\left.+\log(\chi+1)\log\left(\frac{\beta(s)-\chi}{1+\beta(s)}\right)\right)+\frac{1}{2}\left(\mathrm{Li}_2\left(\frac{\chi+1}{2}\right)+\log\left(\frac{1-\chi}{2}\right)\ln(\chi+1)\right)$$

$$+\frac{1}{4}(\log^2(\chi+1))$$

$$+\frac{1}{2}\left(\mathrm{Li}_2\left(\frac{1-\chi}{1-\beta(s)}\right)+\mathrm{Li}_2\left(\frac{1-\chi}{1+\beta(s)}\right)+\log(1-\chi)\log\left(\frac{\chi-\beta(s)}{1-\beta(s)}\right)\right.$$

$$\left.+\log(1-\chi)\log\left(\frac{\chi+\beta(s)}{1+\beta(s)}\right)\right)-\frac{1}{4}\log^2(1-\chi)$$

$$\left.-\frac{1}{2}\left(\mathrm{Li}_2\left(\frac{1-\chi}{2}\right)+\log\left(\frac{\chi+1}{2}\right)\ln(1-\chi)\right)\right].$$

<u>Term D</u>

$$\frac{s}{2}\int_{4m_K^2}^{s-2\sqrt{s}\tilde{\Lambda}} ds' \frac{1}{s-s'}\beta(s')^2 \log\left(\frac{1+\beta(s')}{1-\beta(s')}\right)$$
$$= 4m_K^2 s\left[\int_0^{\chi} d\beta(s')\frac{\beta(s')^3}{1-\beta^2(s')}\frac{1}{\left(s\left(1-\beta^2(s')\right)-4m_K^2\right)}\log\left(1+\beta(s')\right)\right.$$
$$\left.-\int_0^{\chi} d\beta(s')\frac{\beta(s')^3}{1-\beta^2(s')}\frac{1}{\left(s\left(1-\beta^2(s')\right)-4m_K^2\right)}\log\left(1-\beta(s')\right)\right].$$

Again, separating out into terms which are to be partial fractioned gives

$$4m_K^2 s\left[\int_0^{\chi} d\beta(s')\frac{\beta(s')^3}{1-\beta^2(s')}\frac{1}{\left(s\left(1-\beta^2(s')\right)-4m_K^2\right)}\log\left(1+\beta(s')\right)\right.$$
$$\left.-\int_0^{\chi} d\beta(s')\frac{\beta(s')^3}{1-\beta^2(s')}\frac{1}{\left(s\left(1-\beta^2(s')\right)-4m_K^2\right)}\log\left(1-\beta(s')\right)\right]$$
$$= 4m_k^2 s\left[\int_0^{\chi} d\beta(s')\log\left(1+\beta(s')\right)\left(\frac{\beta(s')^3}{1-\beta^2(s')}\frac{1}{\left(s\left(1-\beta^2(s')\right)-4m_K^2\right)}\right)\right.$$
$$\left.-\int_0^{\chi} d\beta(s')\log\left(1-\beta(s')\right)\left(\frac{\beta(s')^3}{1-\beta^2(s')}\frac{1}{\left(s\left(1-\beta^2(s')\right)-4m_K^2\right)}\right)\right].$$

Separating out the bracketed term via partial fractions gives

$$\frac{x^3}{(1-x^2)(s(1-x^2)-4m_K^2)} = \frac{x(4m_K^2-s)}{4m_K^2(4m_K^2+sx^2-s)} + \frac{1}{8m_K^2(x-1)} + \frac{1}{8m_K^2(x+1)},$$

which, apart from a prefactor which will be pulled out of the integral in the first term, is identical to the partial fractioning in term C. This leads to a very high structural similarity and an almost identical result to term C,

$$\frac{s}{2}\int_{4m_k^2}^{s-2\sqrt{s}\tilde{\Lambda}} ds'\,\frac{\beta(s')^2}{s-s'}\log\left(\frac{1+\beta(s')}{1-\beta(s')}\right)$$

$$= 4m_K^2 s\left[\left(\frac{1}{2s}-\frac{1}{8m_k^2}\right)\left(\mathrm{Li}_2\left(\frac{\chi+1}{1-\beta(s)}\right)+\mathrm{Li}_2\left(\frac{\chi+1}{1+\beta(s)}\right)\right.\right.$$

$$+\log(\chi+1)\log\left(-\frac{\chi+\beta(s)}{1-\beta(s)}\right)+\log(\chi+1)\log\left(\frac{\beta(s)-\chi}{1+\beta(s)}\right)\Big)$$

$$+\frac{1}{8m_K^2}\left(\mathrm{Li}_2\left(\frac{\chi+1}{2}\right)+\log\left(\frac{1-\chi}{2}\right)\ln(\chi+1)\right)+\frac{1}{16m_K^2}(\log^2(\chi+1))$$

$$+\left(\frac{1}{8m_k^2}-\frac{1}{2s}\right)\left(\mathrm{Li}_2\left(-\frac{\chi-1}{1-\beta(s)}\right)+\mathrm{Li}_2\left(-\frac{\chi-1}{1+\beta(s)}\right)+\log(1-\chi)\log\left(\frac{\chi-\beta(s)}{1-\beta(s)}\right)\right.$$

$$\left.+\log(1-\chi)\log\left(\frac{\chi+\beta(s)}{1+\beta(s)}\right)\right)-\frac{1}{16m_K^2}\log^2(1-\chi)$$

$$\left.-\frac{1}{8m_K^2}\left(\mathrm{Li}_2\left(\frac{(1-\chi)}{2}\right)+\log\left(\frac{\chi+1}{2}\right)\ln(1-\chi)\right)\right].$$

Term E

$$\int_{4m_K^2}^{s-2\sqrt{s}\tilde{\Lambda}} ds'\,\beta(s') = 8m_K^2\int_0^{\chi} d\beta(s')\frac{\beta(s')^2}{(1-\beta(s')^2)}$$

The general integral of this type is

$$\int_0^{\chi} dx\,\frac{x^2}{(1-x^2)} = \frac{1}{2}\left(-2x+\log\left(\frac{-x-1}{x-1}\right)\right).$$

The results of the integral is therefore

$$\int_{4m_K^2}^{s-2\sqrt{s}\tilde{\Lambda}} ds'\,\beta(s') = 2m_K^2\left[\left(\frac{-2\chi}{\chi^2-1}+\log\left(\frac{1-\chi}{\chi+1}\right)\right)\right].$$

Term F

$$-s\int_{4m_k^2}^{s-2\sqrt{s}\tilde{\Lambda}} ds'\frac{1}{s-s'}\beta(s') = -8m_K^2 s\int_0^{\chi} d\beta(s')\frac{\beta(s')^2}{(1-\beta(s')^2)}\frac{1}{s\left(1-\beta^2(s')\right)-4m_K^2}.$$

Partial fractioning this term is done using the equation

$$\frac{x^2}{(1-x^2)}\left(\frac{1}{s(1-x^2)-4m_K^2}\right)=-\frac{1}{4m_K^2}\frac{1}{(1-x^2)}+\frac{\beta(s)^2}{1-\beta(s)^2}\frac{1}{s(1-x^2)-4m_K^2}.$$

Utilising the equation above gives

$$-s\int_{4m_K^2}^{s-2\sqrt{s}\tilde{\Lambda}}ds'\frac{1}{s-s'}\beta(s')$$
$$=\frac{8m_K^2 s}{\beta(s)}\left[-\frac{1}{4m_K^2}\int_0^{\chi}d\beta(s')\frac{1}{(1-\beta(s')^2)}\right.$$
$$\left.+\frac{\beta(s)^2}{(1-\beta(s)^2)}\int_0^{\chi}d\beta(s')\frac{1}{s(1-\beta^2(s'))-4m_K^2}\right].$$

The first of these integrals has the solution

$$\int_0^{\chi}d\beta(s')\frac{1}{(1-\beta(s')^2)}=\frac{1}{2}\log\left(\frac{1+\chi}{1-\chi}\right).$$

The second integral was solved utilising the equation

$$\int dx\frac{1}{a^2-x^2}=\frac{1}{2a}\log\left|\frac{x+a}{x-a}\right|.$$

Substituting the variables $s-4m_k^2$ and $s\beta(s')^2$ for a and x gives

$$\int_0^{\chi}d\beta(s')\frac{1}{s-4m_k^2-s\beta(s')^2}=\frac{1}{s}\int_0^{\chi}d\beta(s')\frac{1}{\beta(s)^2-\beta(s')^2}=\frac{1}{2\beta(s)s}\log\left|\frac{\sqrt{s}\chi+\sqrt{s-4m_k^2}}{\sqrt{s}\chi-\sqrt{s-4m_k^2}}\right|.$$

This then results in the final solution of the integral of term F

$$-s\int_{4m_k^2}^{s-2\sqrt{s}\tilde{\Lambda}}ds'\frac{1}{s-s'}\beta(s')=\frac{s}{\beta(s)}\left[\log\left(\frac{1+\chi}{1-\chi}\right)-\log\left(\frac{\beta(s)+\chi}{\beta(s)-\chi}\right)\right].$$

Collecting all of the terms together, the final integral then has the form

$$\int_{4m_K^2}^{s-2\sqrt{s}\tilde{\Lambda}}ds'\,\rho_{fin}(s,s')=\frac{2\alpha}{\pi s}[Term\ 1+Term\ 2+Term\ 3],$$

where

$$Term\ 3=Term\ A+Term\ B+Term\ C+Term\ D+Term\ E+Term\ F\ .$$

As a check on the correctness of the integral, the inclusive $\eta(s)$ correction, which is a known function, was compared to the $I(s)$ function as $\widetilde{\Lambda}$ approaches zero. In order to compare the two, one must include the virtual correction terms with the real correction from $I(s)$. This leads one to define the variable

$$\tilde{\eta}(s) \equiv \frac{\pi}{\alpha}\left[\delta_{fin}(\Lambda) + \int_{4m_k^2}^{s-2\sqrt{s}\widetilde{\Lambda}} ds'\, \rho_{fin}(s,s')\right].$$

It is $\tilde{\eta}(s)$ which must be compared with $\eta(s)$ in the limit $\widetilde{\Lambda}$ approaches zero. The virtual term in the $\tilde{\eta}(s)$ function is

$$\delta_{fin}(\Lambda) = \log\left(\frac{2\Lambda}{\sqrt{s}}\right) B_k(s) + \tilde{\delta}_{fin}^{V+S}(s),$$

where

$$B_k(s) = \frac{2\alpha}{\pi}\left[\frac{1+\beta^2(s)}{2\beta(s)}\log\left(\frac{1+\beta(s)}{1-\beta(s)}\right) - 1\right]$$

and

$$\begin{aligned}\tilde{\delta}_{fin}^{V+S}(s) = \frac{\alpha}{\pi}\Bigg\{&\frac{3s-4m_k^2}{s\beta(s)}\log\left(\frac{1+\beta(s)}{1-\beta(s)}\right) - 2 - \frac{1}{2}\log\left(\frac{1-\beta^2(s)}{4}\right) - \frac{3}{2}\log\left(\frac{s}{m_k^2}\right)\\ &- \frac{1+\beta^2(s)}{2\beta(s)}\left[\log\left(\frac{1+\beta(s)}{1-\beta(s)}\right)\left[\log\left(\frac{1+\beta(s)}{2}\right) + \log(\beta(s))\right]\right.\\ &+ \log\left(\frac{1+\beta(s)}{2\beta(s)}\right)\log\left(\frac{1-\beta(s)}{2\beta(s)}\right) + 2\mathrm{Li}_2\left(\frac{2\beta(s)}{1+\beta(s)}\right) + 2\mathrm{Li}_2\left(-\frac{1-\beta(s)}{2\beta(s)}\right)\\ &\left.- \frac{2}{3}\pi^2\right]\Bigg\}.\end{aligned}$$

The Λ used above is of course in our case $\widetilde{\Lambda}$, which I will loosely refer to as Λ during the following checks. The function for the inclusive correction $\eta(s)$ is given by

$$\begin{aligned}\eta(s) = \frac{1+\beta^2(s)}{\beta(s)}\Bigg\{&4\mathrm{Li}_2\left(\frac{1-\beta(s)}{1+\beta(s)}\right) + 2\mathrm{Li}_2\left(-\frac{1-\beta(s)}{1+\beta(s)}\right) - 3\log\left(\frac{2}{1+\beta(s)}\right)\log\left(\frac{1+\beta(s)}{1-\beta(s)}\right)\\ &- 2\log(\beta(s))\log\left(\frac{1+\beta(s)}{1-\beta(s)}\right)\Bigg\} - 3\log\left(\frac{4}{1-\beta^2(s)}\right) - 4\log(\beta(s))\\ &+ \frac{1}{\beta^3(s)}\left[\frac{5}{4}(1+\beta^2(s))^2 - 2\right]\log\left(\frac{1+\beta(s)}{1-\beta(s)}\right) + \frac{3}{2}\left(\frac{1+\beta^2(s)}{\beta(s)^2}\right).\end{aligned}$$

In figure 8 , the log term in $\delta_{fin}(\Lambda)$ (referred to in the figure as Bdfin) and the analytical integral value are plotted as function of lambda, at an s value of 1. The second term in $\delta_{fin}(\Lambda)$, being independent of Λ, is omitted.

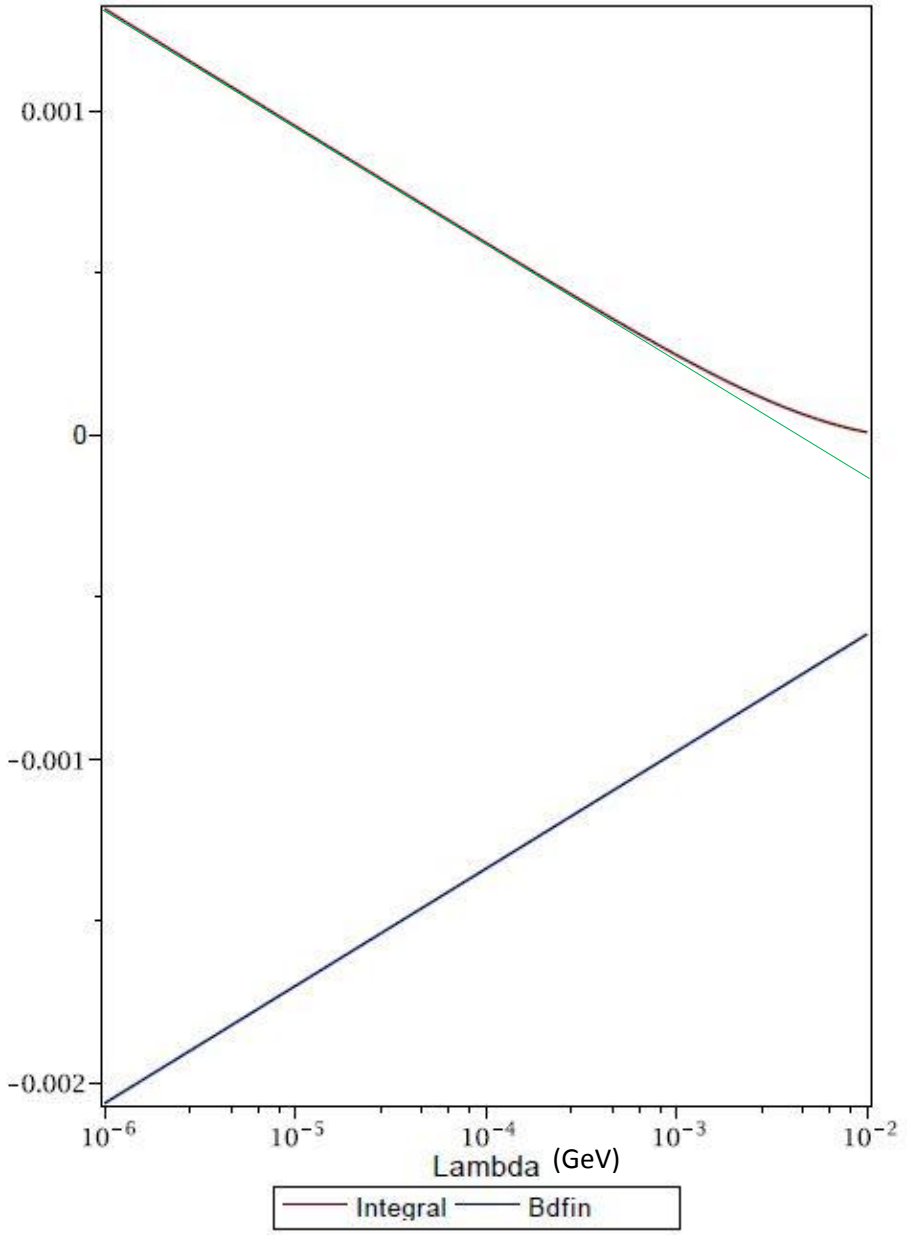

Figure 8: Plot of the integral and Bdfin values as a function of Λ.

The logarithmic term of course appears linear due to the logarithmic scale on the abscissa, whereas the integral curve appears to approach logarithmic behaviour in the limit Λ approaches zero, as shown by the green line. This is to be expected, given the fact that the sum of these two curves must approach a constant in the limit Λ approaches zero, the inclusive eta function being independent of Λ.

In figure 9, the functions $\tilde{\eta}(s)$ and $\eta(s)$ are plotted as a function of Λ, again at an s value of 1. In relation to figure 8, the red line in figure 9 is the sum of the blue and purple lines in figure 8, in other words the eta value with a finite regulator. One can see that the $\tilde{\eta}(s)$ value does indeed approach the inclusive correction value in the limit Λ approaches zero.

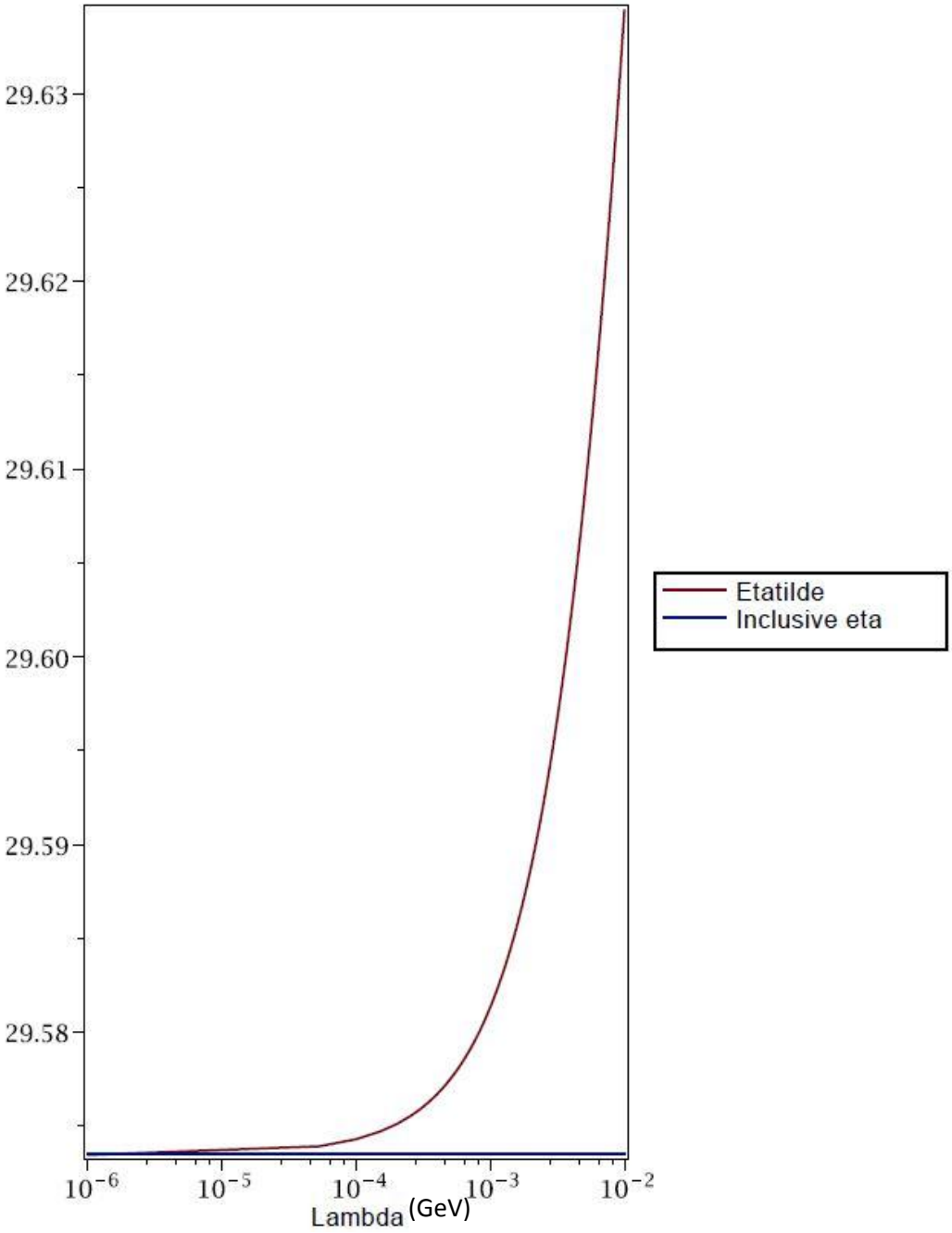

Figure 9: Plot of the η̃(s) and η(s) curves as a function of Λ

As another check, I integrated each term numerically with the use of Maple. Expecting a strong agreement between the two methods due to the fact that the individual terms were simple, one dimensional integrals, this allowed me to spot mistakes (dropped prefactors etc.) This method would not alert me to a mistake I made in breaking the integral up into smaller parts, however, so I added up all the analytically integrated terms and compared

this to the unseperated total numerical integral with original variables, again finding good agreement. These tests therefore gave me confidence that what I had done was correct and so allowed me to move on.

The next step is to decide how the integral is to be deployed. As mentioned above, the $\widetilde{\Lambda}$ value is dependent on the particular experiment, meaning that different experimental cuts made by different experiments will lead to necessarily different $\widetilde{\Lambda}$ values. The below table displays the K+K- literature search for FSR cuts.

Experiment	Mention of FSR corrections	Present in low systematic set	Present in modern set
CMD-2 detector, VEPP-2M Collider, Budker Institute for Nuclear Physics, Novosibirsk		Yes	Yes
SND experiment, VEPP-2M Collider, Budker Institute for Nuclear Physics, Novosibirsk	$\Delta\phi \leq 15°$ for $\sqrt{s} < 1.08$ GeV $\Delta\phi \leq 8°$for 1.08 GeV $\leq \sqrt{s} < 1.1$ GeV $\Delta\phi \leq 5°$for $\sqrt{s} \geq 1.1$ GeV $\Delta\theta \leq 10°$	Yes	Yes
MEA magnetic apparatus, ADONE experiment, Frascati National Laboratory,Rome	$\Delta\phi < 8°$ $\Delta\theta < 10°$	No	No
BCF detector, ADONE experiment, Frascati National Laboratory,Rome		No	No
Magnetic detector DM1, Orsay colliding Beam facility DCI.	"Colinearity within $8°$; this is equivalent to a cut in the missing momentum at 13% of the momentum of the kaons; it determines the maximum photon energy in inelastic radiative effects and	Yes	No

	the amount of radiative corrections to apply.”		
Magnetic detector DM2, Orsay colliding Beam facility DCI.	“The two azimuthal angles equal to within 4 standard deviations” “$5°$ at most in polar angle between the two tracks (to allow for electron radiation).”	Yes	No
DM2 Brighton Conference, DM2 experiment, Orsay colliding Beam facility DCI		No	No
OLYA detector, VEPP-2M Collider, Budker Institute for Nuclear Physics, Novosibirsk	“For the first experiment it was also required that the spatial acolinearity angle was less than $30°$, while for the second one the requirements were more strict because of the smaller multiple scattering: $\Delta\phi \leq 10$ $\Delta\theta < 10°$ ”	No	No
Neutral Detector, VEPP-2M Collider, Budker Institute for Nuclear Physics, Novosibirsk		No	Yes

CMD-2 detector, VEPP-2M Collider, Budker Institute for Nuclear Physics, Novosibirsk	"The azimuthal angle difference ($\Delta\phi$) is less than 0.1 radian"	Yes	Yes
SND experiment, VEPP-2M Collider, Budker Institute for Nuclear Physics, Novosibirsk	"Acolinearity in the azimuthal plane $\Delta\phi < 10°$"	Yes	Yes

Table 8: Literature search of FSR corrections types and whether or not they are present in the Low Systematic and Modern custom sets. The angles are the conventional angular spherical coordinates.

4.3 Relation between experimental acollinearity cuts and FSR correction

One type of experimental cut to consider is the acolinearity cut. This demands that the final state particles, in this case kaons, are measured to be back-to-back. An angle is then chosen as the acolinearity cut off; any pair of particles which differ in their direction of flight by more than this angle are discarded as not being created in the same event, or particles which are constituents of a final state one is not measuring. While this cut is important to prevent the accidental pairing of two uncorrelated background particles, it necessarily means some data will be discarded. For instance, in the process

$$e^+ + e^- \rightarrow \gamma^* \rightarrow K^+ + K^- + \gamma$$

the emitted photon will change the direction of the kaon from which it was emitted. The final state particles are all real and on mass shell, meaning that there are no unconstrained momenta and four-vector kinematics may be used to calculate the energy of the emitted photon, as a function of the angle at which it was emitted. In this way, an angular cut is in some way equivalent to an energy cut on the final state photon. In order to calculate this relationship, one starts with the equation

$$\vec{p}_\gamma = \vec{p}_f - \vec{p}_i$$

expressing the conservation of three momentum at the photon emission vertex, $\vec{p}_\gamma$ being the photon three momentum and $\vec{p}_i(\vec{p}_f)$ representing the initial (final) three momentum of the final state, photon-emitting kaon. Squaring both sides gives

$$p_\gamma^2 = \left(\vec{p}_f - \vec{p}_i\right)^2 = {\vec{p}_f}^2 + {\vec{p}_i}^2 - 2\vec{p}_f \cdot \vec{p}_i \ .$$

Using the relation

$$\left|\vec{p}_\gamma\right| = E_\gamma$$

and the small angle assumption

$$\vec{p}_f \approx \vec{p}_i \equiv \vec{p}_\parallel \ ,$$

the equation for conservation of three momenta becomes

$${E_\gamma}^2 = 2{p_\parallel}^2 - 2{p_\parallel}^2 cos\Omega \ ,$$

where Ω in the above equation represents the angle between the two three vectors. Rearranging and inserting the on shell energy momentum relationship gives

$$E_\gamma{}^2 = 2p_\parallel{}^2(1 - cos\Omega) = 2\left(E_\parallel{}^2 - m_K^2\right)(1 - cos\Omega).$$

$E_\parallel$ is the energy of one of the kaons produced in the collision which is half of the centre of mass energy. Inserting this gives

$$E_\gamma = \sqrt{2\left(\left(\frac{\sqrt{s}}{2}\right)^2 - m_K^2\right)(1 - cos\Omega)} = \sqrt{2\left(\frac{s}{4} - m_K^2\right)(1 - cos\Omega)}.$$

This equation therefore relates the acolinearity angle with the energy of a photon which would be produced in this process. The key is therefore that, by relating the angular cut used in the experiment to an energy cut, one can use the integral $I(s)$, with the energy E_γ being used as the specific regulator $\widetilde{\Lambda}$ for those experiments which make acolinearity cuts. This gives the final equation

$$\widetilde{\Lambda} = \sqrt{2\left(\frac{s}{4} - m_K^2\right)(1 - cos\Omega)}.$$

4.4 Application of experimentally adjusted FSR correction to K+K- channel

Referring to the literature table on page 55, one can see that there are three types of cuts, a general acolinearity cut, a cut specifying upper and lower limits on one or both of the angles associated with the coordinate system of the beam, and a cut on the standard deviation of one kaon angle from the other. The third type is not dealt with in this thesis (because those data sets which employ a cut of this kind are off the phi peak and thus of diminished relative importance), but the first can be straightforwardly related to the equation derived in the previous section, as the angle specified in the equation relating the angle to the experiment dependant regulator is the angle between the three-vectors of the initial particles, which is precisely the acollinearity parameter. The only experiment which utilises this type of cut is the DM1 magnetic detector. A comparison between the correction factor which utilises the whole inclusive final state correction, plus or minus one half the value, henceforth referred to as C_{FSR}(Old), and the experiment dependant correction factor found using the integral, henceforth called C_{FSR} (New), are shown below.

Energy Range (GeV)	Mean Energy Value (MeV)	C_{FSR}(New)	C_{FSR}(Old)
1.4-1.449	1.4245	1.003557 $\pm$ 0.003557	1.012 $\pm$ 0.00603
1.45-1.485	1.4675	1.00392 $\pm$ 0.00392	1.0116 $\pm$ 0.005806
1.5-1.549	1.5245	1.004388 $\pm$ 0.004388	1.0111 $\pm$ 0.00556
1.55-1.599	1.5745	1.00478$\pm$ 0.00478	1.0107$\pm$ 0.005372
1.6-1.619	1.6095	1.00506 $\pm$ 0.00506	1.0105$\pm$ 0.0052690
1.62-1.639	1.6295	1.00521$\pm$ 0.00521	1.0104$\pm$ 0.00520
1.64-1.659	1.6495	1.00536$\pm$ 0.00536	1.0103$\pm$ 0.00514
1.66-1.679	1.6695	1.00551 $\pm$ 0.00551	1.0102$\pm$ 0.00509
1.68-1.699	1.6895	1.00565$\pm$ 0.00565	1.010$\pm$ 0.00504
1.7-1.729	1.7145	1.00583$\pm$ 0.00583	1.001$\pm$ 0.00498
1.73-1.759	1.7445	1.00605$\pm$ 0.00605	1.0098$\pm$ 0.0049
1.76-1.799	1.7795	1.00629 $\pm$ 0.00629	1.00968 $\pm$ 0.00484
1.8-1.849	1.8245	1.0065967$\pm$ 0.0065967	1.0095$\pm$ 0.00476
1.85-1.929	1.8895	1.00702 $\pm$ 0.0702	1.0093 $\pm$ 0.00465
1.93-1.9925	1.96125	1.00748$\pm$ 0.00748	1.0091$\pm$ 0.004548
2.0-2.06	2.03	1.007897 $\pm$ 0.007897	1.0089$\pm$ 0.00446

Table 9: Comparison between previously used and new experimentally based correction factors for the DM1-DCI experiment.

The errors on the new correction factors have been taken to be 100%. Even with these conservative errors, the ratio between old and new errors is 1.5 at the lowest energy value. As the energies get higher, the errors approach one another, crossing at approximately 1.63 GeV, and then at higher energies the old FSR corrections errors become the smaller of the two. This is not a problem, however, because the anomalous magnetic moment is proportional to the cross section for $e^+e^- \rightarrow \gamma^* \rightarrow K^+K$, which is small for this set due to it being off peak (see figure 5), and at higher energies moves even further away from the resonance and so becomes even smaller. Ideally, we want to apply this method to those data sets which sit on or near the phi peak, where both the contributions to the anomalous magnetic moment will be appreciable and the ratio of the uncertainties between the old and new FSR corrections will be much greater. This area is of course also the region in which the assumptions we have made best approximate the full physical description.

In order to use the equation derived above relating acollinearity to an energy cut, one must relate the acollinearity angle Ω, to the angular spherical coordinates θ and ϕ. The line element in spherical coordinates on a sphere of constant radius r is

$$\Delta s^2 = r^2(\Delta\theta^2 + sin^2\theta\Delta\phi^2).$$

The equation

$$\frac{\Delta s}{r} = \Omega$$

relates the line element to the combined azimuthal and polar angles, the angle which diagonally spans the solid angle. This is precisely the angle between the three-vectors, Ω, which was defined earlier to be the acollinearity angle. Inserting the above equation into the line element formula gives

$$\Omega = \sqrt{\Delta\theta^2 + sin^2\theta\Delta\phi^2}.$$

The value of θ is unknown, but the range in the acollinearity as the polar angle varies is

$$\Delta\theta \leq \Omega \leq \sqrt{\Delta\theta^2 + \Delta\phi^2}.$$

Referring to the above literature table (table 8), one can see that the angular cuts imposed span the range 5-10 degrees. Taking the small angle approximation of the equation

$$\frac{E_\gamma}{|p_\parallel|} = \sqrt{2(1 - cos\Omega)}$$

gives

$$\frac{E_\gamma}{|p_\parallel|} = \sqrt{2\left(1 - \left(1 - \frac{\Omega^2}{2}\right)\right)} = \Omega.$$

Inserting the energy-momentum relation and rearranging gives

$$\mathrm{E_\gamma} = \Omega\left(\frac{\mathrm{s}}{4} - \mathrm{m_K^2}\right).$$

Using this equation and the range in the acollinearity, one can say that the range in the experimental regulator is

$$\Delta\theta\left(\frac{\mathrm{s}}{4} - \mathrm{m_K^2}\right) \leq \widetilde{\Lambda} \leq \sqrt{\Delta\theta^2 + \Delta\phi^2}\left(\frac{\mathrm{s}}{4} - \mathrm{m_K^2}\right).$$

Due to the small angle approximation which the data sets tend to obey, the interval between these two extremes will be small. One may therefore take the $\widetilde{\Lambda}$ value to be the mean

$$\widetilde{\Lambda} = \left(\frac{\mathrm{s}}{8} - \frac{\mathrm{m_K^2}}{2}\right)\left[\sqrt{\Delta\theta^2 + \Delta\phi^2} + \Delta\theta\right].$$

Another reason one may take the mean value is that, for angles between 5-10 degrees, the $\widetilde{\Lambda}$ values are small enough that, to the required accuracy, a factor of 2 or 3 between values is unimportant. This is shown by the graph below.

Only one data set in table 8 employs a cut on two angles, the data from the SND experiment. The table below displays the old and new FSR correction, the new corrections using the method detailed above.

Energy Range (GeV)	C_{FSR}(New)	C_{FSR}(Old)
1.04	1.0007418 $\pm$ 0.0007418	1.033159 $\pm$ 0.01658
1.05	1.000871 $\pm$ 0.000871	1.03037 $\pm$ 0.01518
1.06	1.0009967 $\pm$ 0.0009967	1.0280 $\pm$ 0.0141
1.07	1.00112 $\pm$ 0.00112	1.0260 $\pm$ 0.0132
1.08	1.001427 $\pm$ 0.001427	1.0250 $\pm$ 0.01247
1.09	1.001560 $\pm$ 0.001560	1.0237 $\pm$ 0.01185
1.10	1.0017756 $\pm$ 0.001776	1.0226 $\pm$ 0.01132
1.11	1.001910 $\pm$ 0.001910	1.0217 $\pm$ 0.01085
1.12	1.0020419 $\pm$ 0.0020419	1.0209 $\pm$ 0.01044
1.13	1.002170 $\pm$ 0.002170	1.0201 $\pm$ 0.010
1.14	1.002295 $\pm$ 0.002295	1.0195 $\pm$ 0.00975
1.15	1.002417 $\pm$ 0.002417	1.0189 $\pm$ 0.00945
1.16	1.002537 $\pm$ 0.002537	1.01837 $\pm$ 0.009186
1.18	1.00277 $\pm$ 0.00277	1.0174 $\pm$ 0.0087
1.19	1.002878$\pm$ 0.002878	1.017 $\pm$ 0.0085
1.20	1.00298 $\pm$ 0.00298	1.0166 $\pm$ 0.00832

The above table only shows the data up to 1.2 GeV, in other words the data not on the peak is not included. The ratio of old and new errors is shown graphically below.

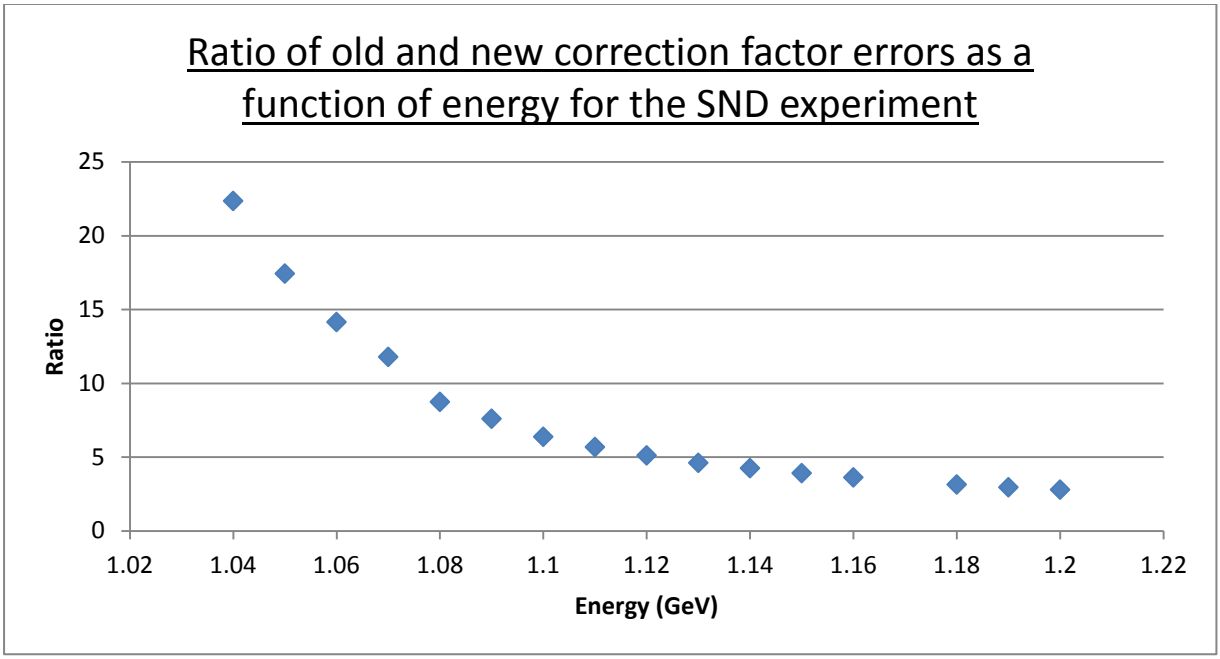

Figure 10: This graph shows how the ratio of old to new correction factor errors changes as a function of energy. Note that the phi peak is around 1.02 GeV, meaning that most of the above data points are quite far away from the resonance.

One can see that there is a large reduction of the errors using this method, a reduction which is most prominent for data close to the phi peak.

Another type of cut employed by the experiments in the K+K- channel is a cut purely in the azimuthal angle. This reduces the geometry to transverse variables in the x-y plane. If one makes the assumption that the ratio between the photon energy and the momentum of the radiating kaon is approximately independent of direction, one may set up the relation

$$\frac{E_\gamma}{\vec{p}_\parallel} \approx \frac{E_\gamma^{\mathrm{T}}}{\vec{p}_\parallel^{\mathrm{T}}},$$

where the superscript T denotes that the variables are the components of those observables in the plane transverse to the beam. This allows one to convert the equation relating energy to general acollinearity for the case where only one angular cut is given

$$\frac{E_\gamma^{\mathrm{T}}}{\vec{p}_\parallel^{\mathrm{T}}} = \sqrt{2(1-cos\Delta\phi)}.$$

and replace the specifically transverse variables with their general versions

$$\frac{E_\gamma}{\vec{p}_\parallel} \approx \sqrt{2(1-cos\Delta\phi)}.$$

Expanding the above equation out using the small angle approximation gives

$$\frac{E_\gamma}{\vec{p}_\parallel} \approx \sqrt{2\left(1-\left(1-\frac{(\Delta\phi)^2}{2}\right)\right)} = \Delta\phi.$$

The equation relating the regulator $\widetilde{\Lambda}$ to the azimuthal angular cut is therefore

$$\widetilde{\Lambda} \approx \vec{p}_\parallel\sqrt{2(1-cos\Delta\phi)} = \sqrt{2(E_\parallel^2 - m_K^2)(1-cos\Delta\phi)} = \sqrt{2\left(\frac{s}{4}-m_K^2\right)(1-cos\Delta\phi)},$$

which in the small angle approximation simplifies to

$$\widetilde{\Lambda} \approx \sqrt{\left(\frac{s}{4}-m_K^2\right)}\,\Delta\phi.$$

Table 8 shows that there are three experiments which employ this type of correction, the CMD-2 experiment and both scans of the SND experiment. These data sets also lie much closer to the peak than those previously analysed. The data for the CMD-2 experiment is shown below.

Energy Range (GeV)	C_{FSR}(New)	C_{FSR}(Old)
1.008624	1.000065011 $\pm$ 0.000065011	1.05263 $\pm$ 0.026315
1.013882	1.000098572 $\pm$ 0.000098572	1.047 $\pm$ 0.0235
1.016726	1.00011837 $\pm$ 0.00011837	1.0446 $\pm$ 0.0223
1.017264	1.00012223 $\pm$ 0.00012223	1.0442 $\pm$ 0.0221
1.017654	1.00012506 $\pm$ 0.00012506	1.04392 $\pm$ 0.02196
1.017934	1.00012709 $\pm$ 0.00012709	1.04372 $\pm$ 0.02186
1.017992	1.00012752 $\pm$ 0.00012752	1.043675 $\pm$ 0.021838
1.018322	1.00012993 $\pm$ 0.00012993	1.04344 $\pm$ 0.02172
1.018806	1.0001335 $\pm$ 0.0001335	1.0431 $\pm$ 0.02155
1.01907	1.00013545 $\pm$ 0.00013545	1.0429 $\pm$ 0.02145
1.019468	1.00013842 $\pm$ 0.00013842	1.04264 $\pm$ 0.02132
1.019636	1.00013968 $\pm$ 0.00013968	1.04253 $\pm$ 0.021265
1.021762	1.00015585 $\pm$ 0.00015585	1.04116 $\pm$ 0.02058
1.022072	1.00015825 $\pm$ 0.00015825	1.040976 $\pm$ 0.020488
1.027996	1.0002059 $\pm$ 0.0002059	1.0378 $\pm$ 0.0189

One can see immediately that this data set is much closer to the phi peak, and so greater improvements in the errors would be expected. This ratio of the errors is shown below.

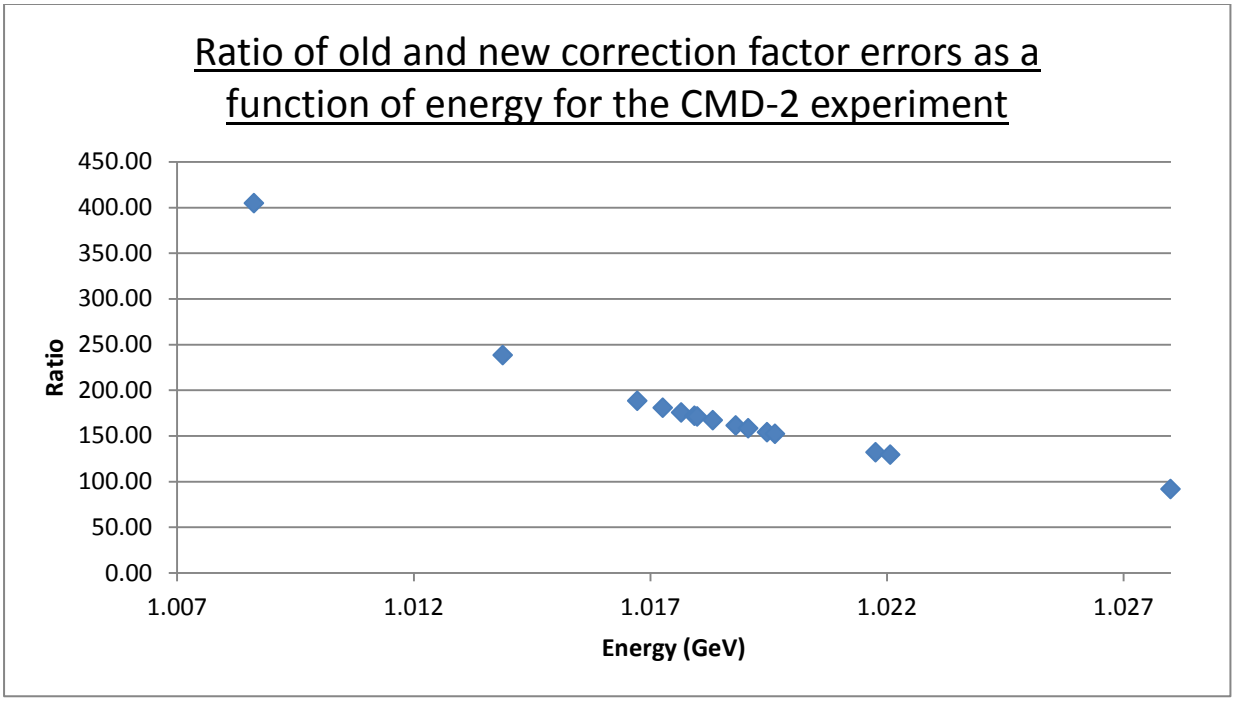

Figure 11: Graph displaying ratio of old to new correction factor errors as a function of energy for the CMD-2 experiment. This data is much closer to the peak and shows a reduction of errors in the phi peak region by approximately 2 orders of magnitude.

One can see that the errors have been reduced by up to two orders of magnitude in this range. Similarly for both of the SND scans, the graph displaying the ratio of errors is shown below (the data tables are in Appendix 1).

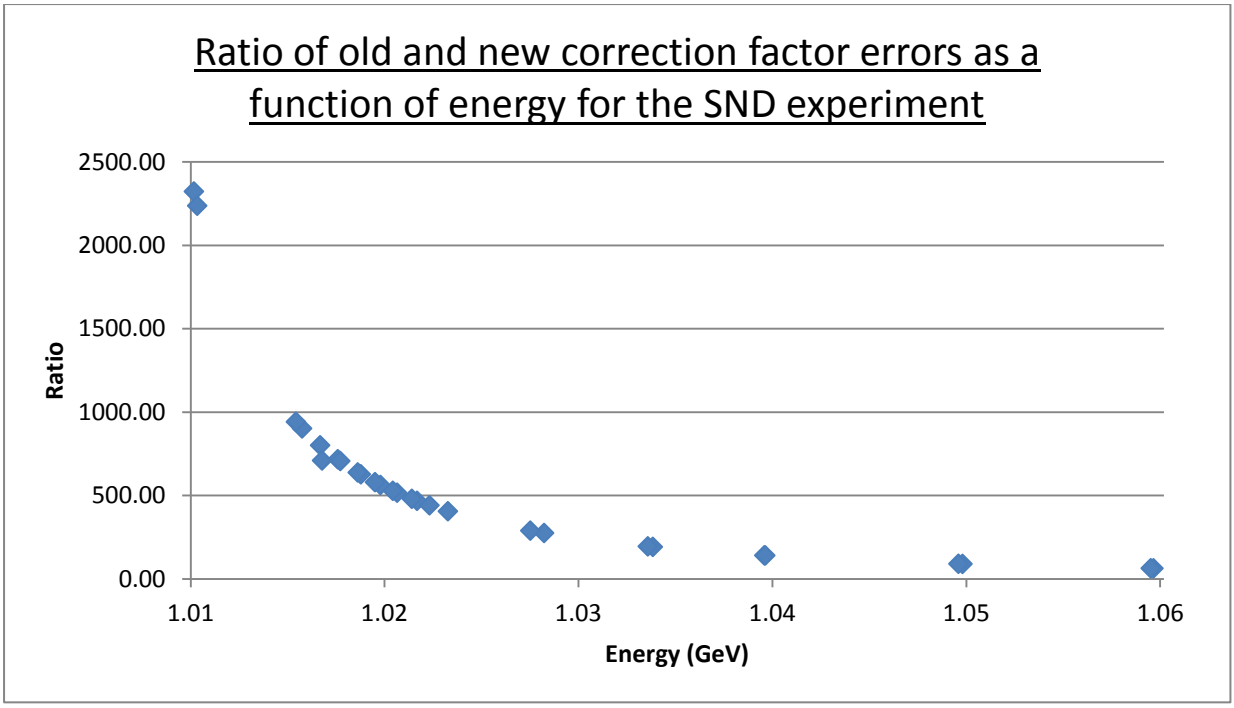

Figure 12: Graph displaying the ratio of old and new correction factor errors as a function of energy for the SND experiment. This table displays the information from scans both 1 and 2.

The improvement ranges from a factor of approximately 2500 at about 1.01 GeV, to a factor of about 50 near 1.06 GeV. One can see clearly from this that, close to the phi peak where the cross section for the creation of a K+K- pair is substantial, one achieves a greater improvement in the uncertainties, in this case even reducing the errors by as much as 3 orders of magnitude in some energy regions.

One can see from the data tables that utilising this method does not just reduce the uncertainties associated with the correction factors, but the values of the correction factors themselves. Plotting the ratio of the difference from unity of the old and new correction, in other words the ratio

$$R = \frac{\eta(s)_{old}}{\eta(s)_{new}},$$

for the SND experiment gives the graph below.

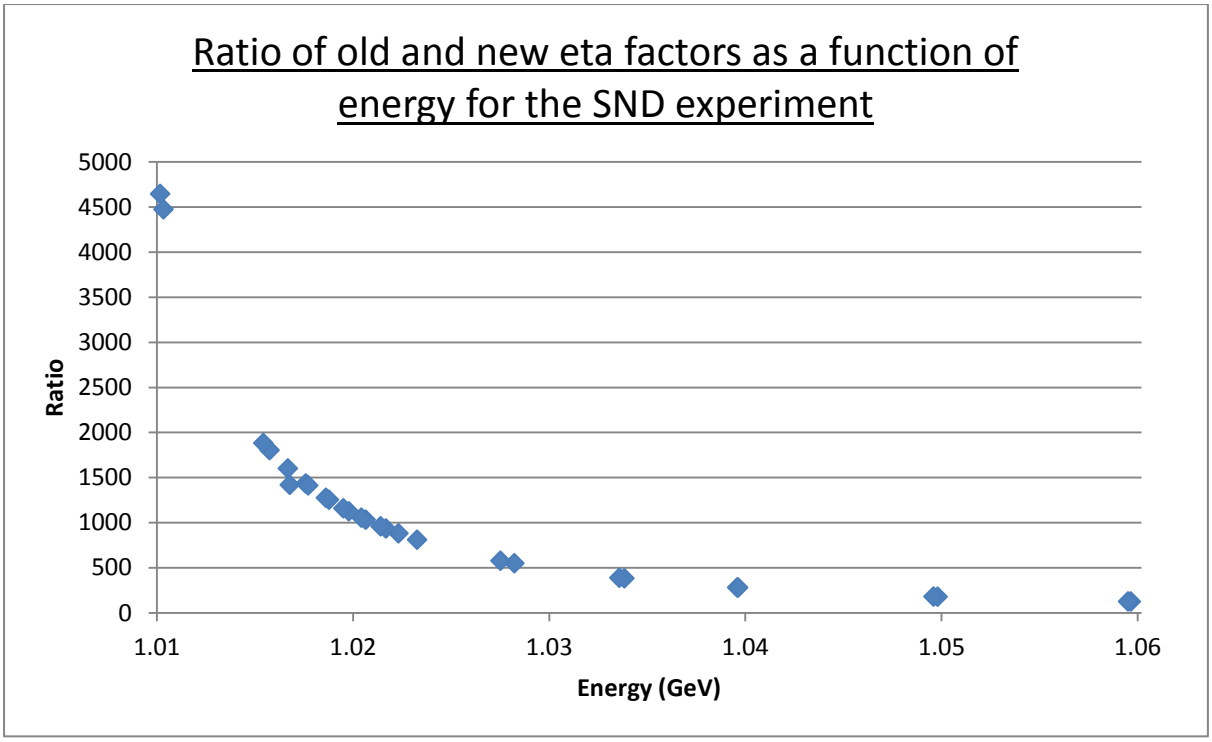

Figure 13: Graph displaying the ratio of the old and new eta factors for the SND experiment. The eta factor is simply the deviation from unity of the correction factor.

The above graph displays eta rather than the correction factor to stress the size difference between the old and new FSR corrections. One can see that at low energies the ratio is of the order of 10^3, meaning that at these energies, the amount of hard radiation is much less than was previously being accounted for. The ratio of the full correction factors is shown below.

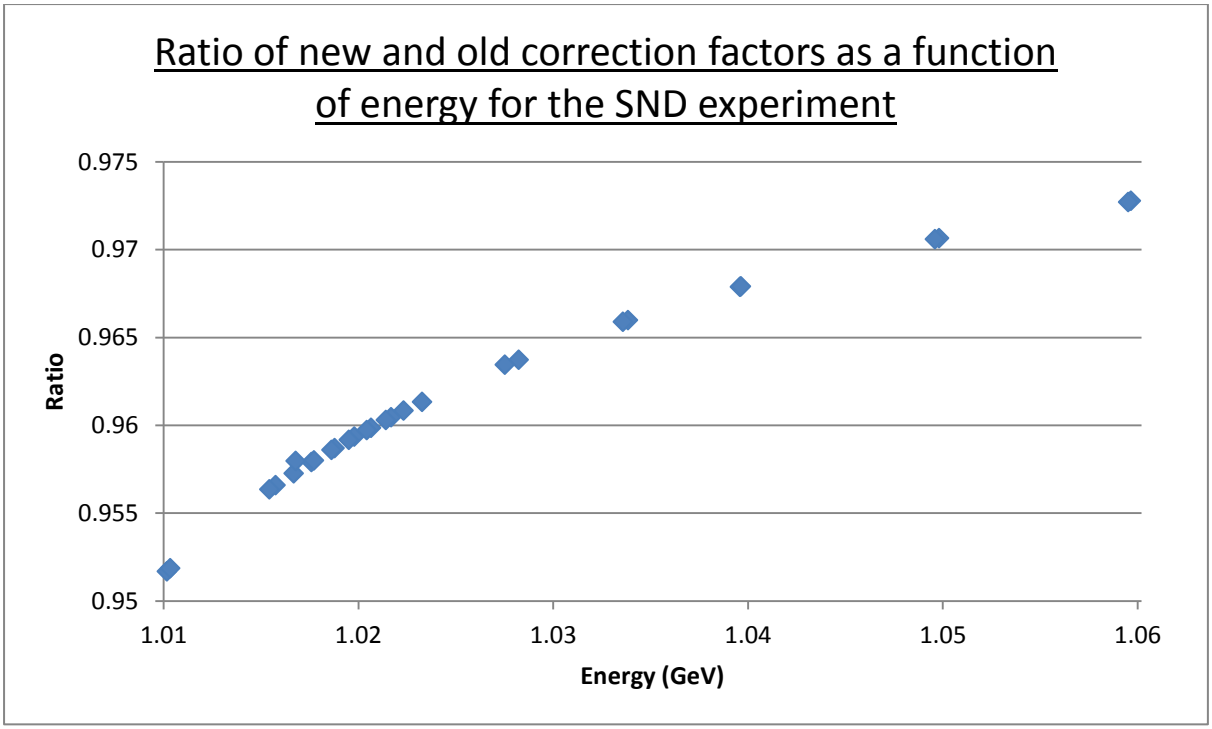

Figure 14: Graph displaying the ratio of the new and old correction factors for the SND experiment.

The above graph shows that, at the phi peak around 1.02 GeV, the correction factor is only about 96% of its previous value. This means that, because the correction factor inflates the cross section to include FSR contributions, a smaller correction factor will lead to a smaller cross section and hence a smaller anomalous moment via the dispersion relation. The fact that the cross section is much larger on the phi peak and the peak is symmetric around 1.02 GeV would suggest that a reduction of approximately 4% would be expected in the K^+K^- channel anomalous moment contribution. This would result in a reduction of the leading order hadronic contribution to the total anomalous magnetic moment value of around 0.14%.

It is worth reiterating at this point that the discrepancy between theory and experiment is (4)

$$a_\mu^{exp} - a_\mu^{SM} = (26.1 \pm 8.0) \cdot 10^{-10}.$$

The experimental value is therefore larger than that currently predicted using the standard model. The application of the new correction factor makes the anomalous moment smaller, and hence increasing the discrepancy.

Chapter 5

Possible explanations for discrepancy between theory and experiment

At the present time, the disparity between the theoretical calculations of the anomalous magnetic moment of the muon using the standard model and the experimentally measured value is around 3 σ. There are three possible explanations for this difference. The first is that some theoretical effect or mistake has been overlooked. This is still possible, although as a greater number of independent groups verify the discrepancy, the likelihood of this explanation decreases. The second possibility is that the deviation is an experimental fluctuation. 3 σ corresponds to a 0.27% chance of this which, while small, is not small enough to be confidently ruled out. It is one of the aims of the E989 experiment to rule this possibility out. The third reason is that new physics which has not been included in the standard model calculation is affecting the measured value of the anomalous moment. There are other physical reasons, such as dark matter and the naturalness problem, for believing that the standard model does not exhaustively list all of the particles found in nature, and both the omission of gravity and the mechanism for neutrino oscillations from the standard model shows that it is at least incomplete. A statistically significant deviation measurement would therefore be a clear sign of new physics, examples of which are now discussed.

The simplest and least radical method of extending the standard model would be to add what are called sequential fermions. These are members of a fourth generation of quarks and leptons, with the same quantum numbers as the other three but constrained to have a neutrino mass of greater than half the mass of the Z boson. One manifestation of such an extension is predicted to affect the decay rate of the virtual Higgs boson into a pair of photons (28). It is known, however, that sequential fermions could not explain the total discrepancy. This is because the contribution from new physics to the anomalous moment takes the form

$$a_\mu^{NP} = C\frac{m_\mu^2}{M_{NP}^2},$$

where C is some constant of order α/π and M_{NP} is the mass of the particle or resonance associated with the new physics. The lower limit as set by experiment on the mass of a fourth generation fermion is approximately 100 GeV (31) (32), which leads to a contribution of about 1.34×10^{-13}. This is tiny compared to the discrepancy of 4.2×10^{-10}, showing that sequential fermions alone cannot be a satisfactory extension to the standard model.

Another possibility is the two-Higgs-doublet model (2HDM) (31) (33). The standard model assumes the simplest possible Higgs mechanism, that which acts via a single scalar Higgs field. The 2HDM is a possible alternative, where an extra Higgs field (also sometimes referred to as a Higgs doublet) is added, resulting in the addition of four more scalar particles; an additional neutral scalar, a neutral pseudoscalar, and two charged bosons $H^{\pm}$. Measurements of decay rates and branching ratios will be used to experimentally verify whether or not the standard model utilises a minimal Higgs mechanism.

A more popular and more radical extension of the standard model is Supersymmetry. Supersymmetry postulates that every particle in the standard model has a supersymmetric particle which differs by half a unit of spin. Cancellations between the quantum corrections from the particles of the standard model and their superpartners help resolve some unanswered questions in modern physics, such as why the mass of the Higgs is not close to the Planck mass. The existence of such particles would lead to a supersymmetric contribution to the anomalous moment and hence could be the source of the discrepancy.

The contribution to the anomalous moment from a new interacting particle is given by

$$\delta a_\mu = O(C)\left(\frac{m_\mu}{\Lambda}\right)^2 \quad , \quad C = \frac{\delta m_\mu}{m_\mu}$$

where δa_μ is the change in the anomalous moment from the new particle, δm_μ is the change in the mass of the muon due to the corrections from the new particle, m_μ denotes the mass of the muon and Λ is the energy scale of the new physics. The model dependence of this equation sits entirely within the C factor. A consequence of this equation is that new physics (of this nature) can explain the current discrepancy only if Λ is at the TeV scale or smaller. The correction from SUSY contributions to the anomalous moment is slightly modified to

$$\delta a_\mu = O(C)\left(\frac{m_\mu}{\Lambda}\right)^2 \tan(\beta)\ \mathrm{sign}(\mu),$$

where β denotes the ratio of the two Higgs field vacuum expectation values and μ is the Higgsino mass parameter. A numerical approximation to the above equation using current SUSY models gives

$$\delta a_\mu \approx 13 \times 10^{-10}\left(\frac{100\ GeV}{\mathrm{M_{SUSY}}}\right)^2 \tan(\beta)\ \mathrm{sign}(\mu).$$

This approximation is completely valid when all of the SUSY particles have the mass $\mathrm{M_{SUSY}}$. This shows that, for SUSY masses of 200 GeV and $\tan(\beta)\sim 10$ or SUSY masses 500 GeV and $\tan(\beta)\sim 50$, the known discrepancy could be easily explained (29). The LHC has experimentally ruled out squarks up to around 1 TeV (34), but sleptons are not yet so tightly constrained (35).

Conclusion

The investigations within this project have revealed several pieces of information in relation to the calculation of leading order hadronic contributions to the anomalous magnetic moment of the muon. The removal of certain data sets was found to significantly reduce the uncertainty on the calculation of the anomalous moment. This leads one to the conclusion that some of the different sets are incongruous. One must then give preference to those sets with relatively small errors. Taking this strategy with regard to selection of sets within the K+K- channel, a reduction of the error on the anomalous magnetic moment of approximately 20% was found, for $\sqrt{s} \sim 1$ GeV.

Another finding was with regards to the amount of final state radiative corrections that were required to be applied to the measured cross section. The initial conservative route was to take half the inclusive eta factor value, with an uncertainty of plus or minus a half of that value, as displayed below.

$$C_{fsr} = \left(1 + 0.5\,\eta(s)\frac{\alpha}{\pi}\right) \pm 0.5\,\eta(s)\frac{\alpha}{\pi},$$

where $\eta(s)$ is inclusive, in other words includes all real, virtual and soft radiative corrections. By relating the experimental cuts employed by each individual experiment in the K+K- channel to the experimentally dependant regulator $\widetilde{\Lambda}$, one could perform the calculation of the FSR correction factor for each experiment. One consequence of applying this process to the K+K- channel was that the amount of correction was found to be largely negligible close to the phi peak, with the correction factors being the same as unity to an accuracy of a few parts in 10^4 or 10^5. As shown by the equation

$$\sigma_{fin} = \left(1 + \eta(s)\frac{\alpha}{\pi}\right)\sigma_0\,,$$

the reduction of the correction factor will reduce the bare cross section used in the dispersion relation and hence lower the calculated value of the anomalous magnetic moment. This is especially true because those energies for which the cross section is greatest and hence contribute more, in other words the energies on and around the phi peak, are also around those energies for which the difference between the old and new correction factors is greatest. Taking the phi peak to be around 1.02 GeV, one can say that

the ratio between the old and new correction factors is around 1.04, meaning that the cross section is reduced to 96% of its former value, with a similar decrease expected in the value of the leading order K^+K^- contribution to the anomalous moment. Physically, this shows that the hard final state radiation emitted by the hadrons is much less than previously accounted for. This change in the anomalous moment makes the discrepancy between theoretical and experiment values greater.

With regards to reduction of errors, the errors on and around the phi peak were reduced by approximately 2 orders of magnitude, with those in the SND experiment for example reduced by a factor of about 500. The errors on the new correction factors were taken to be 100%. Improvement of this figure will require further investigation into the assumptions made in relating $\widetilde{\Lambda}$ to the angular cuts.

The next steps in this vein of inquiry would be to investigate the assumptions and relations which go into equating the experimentally dependant regulator with the angular cuts. One may also need to find a way to express $\widetilde{\Lambda}$ in terms of the number of standard deviations between the angles of the two Kaons, as used by the DM2 experiment (see table 8). When one was sufficiently confident in the assumptions made, or of course found other perhaps preferable ways to express $\widetilde{\Lambda}$ as a function of the acollinearity angles, one could then apply this method to other hadronic channels, and finally recalculate the anomalous moment to observe the difference this procedure has made to both the value and the associated error of the anomalous magnetic moment of the muon.

Appendices

Appendix 1: Data tables for scans 1 and 2 published by the SND experiment

Energy Range (GeV)	C_{FSR}(New)	C_{FSR}(Old)
1.01017	$1.00001093 \pm 0.00001093$	1.050778 ± 0.025389
1.01575	$1.000025153 \pm 0.000025153$	1.0454 ± 0.0227
1.01668	$1.000027877 \pm 0.000027877$	1.04467 ± 0.022335
1.01759	$1.000030629 \pm 0.000030629$	1.04397 ± 0.021985
1.01878	$1.000034354 \pm 0.000034354$	1.04311 ± 0.021555
1.01979	$1.000037622 \pm 0.000037622$	1.0424 ± 0.0212
1.02065	$1.000040481 \pm 0.000040481$	1.04186 ± 0.02093
1.02168	$1.00004399 \pm 0.00004399$	1.04121 ± 0.020605
1.02327	$1.000049594 \pm 0.000049594$	1.04027 ± 0.020135
1.02823	$1.000068385 \pm 0.000068385$	1.0377 ± 0.01885
1.03384	$1.000091788 \pm 0.000091788$	1.0353 ± 0.01765
1.03959	1.0001178 ± 0.0001178	1.0333 ± 0.01665
1.04981	$1.00016853 \pm 0.00016853$	1.0304 ± 0.0152
1.05966	1.0002218 ± 0.0002218	1.0282 ± 0.0141

Energy Range (GeV)	C_{FSR}(New)	C_{FSR}(Old)
1.01034	1.000011304 $\pm$ 0.000011304	1.05058 $\pm$ 0.02330
1.01543	1.0000242379 $\pm$ 0.0000242379	1.04566 $\pm$ 0.0228
1.01678	1.0000309058 $\pm$ 0.0000309058	1.0439 $\pm$ 0.02195
1.01772	1.000031029 $\pm$ 0.000031029	1.04387 $\pm$ 0.02194
1.01862	1.000033845 $\pm$ 0.000033845	1.04322 $\pm$ 0.0216
1.01951	1.000036707 $\pm$ 0.000036707	1.0426 $\pm$ 0.0213
1.02043	1.000039745 $\pm$ 0.000039745	1.0420 $\pm$ 0.021
1.02141	1.00004306 $\pm$ 0.00004306	1.04138 $\pm$ 0.02069
1.02232	1.00004622 $\pm$ 0.00004622	1.0408 $\pm$ 0.0204
1.02752	1.00006538 $\pm$ 0.00006538	1.0380 $\pm$ 0.0190
1.03358	1.000090657$\pm$ 0.000090657	1.0354 $\pm$ 0.0177
1.03964	1.000118 $\pm$ 0.000118	1.03327 $\pm$ 0.01664
1.04960	1.0001674 $\pm$ 0.0001674	1.03046$\pm$ 0.01523
1.05952	1.000221 $\pm$ 0.000221	1.028277 $\pm$ 0.01414

Bibliography

1. F.Schwabl; "*Advanced Quantum Mechanics";* Springer; 2008.

2. V. B. Berestetskii, O. N. Krokhin, A. X. Klebnikov; **Zh. Eksp. Teor. Fiz. 30 788**; 1956.

3. T. Aoyama, M. Hayakawa, T. Kinoshita, and M. Nio; "*Quantum electrodynamics calculation of lepton anomalous magnetic moments: Numerical approach to the perturbation theory of QED";* **Prog. Theor. Exp. Phys. (2012) 01A107 doi: 10.1093/ptep/pts030;** 2012**.**

4. K. Hagiwara, R. Liao, A.D. Martin, D. Nomura and T. Teubner; "*(g-2)_mu and alpha(M_Z^2) re-evaluated using new precise data.";* **J.Phys. G38 (2011) 085003**, 2011.

5. T. Teubner, K. Hagiwara, R. Liao, et al; *"Update of the g-2 of the muon and delta alpha"***; arXiv:1001.5401;** 2010.

6. *g-2* Online; "*The Brookhaven muon storage ring magnet*" ; **http://www.g-2.bnl.gov/publications/magnet_paper.pdf;** 2001.

7. Joint accelerator conferences website; "*Magnetic field shimming, measurement and control for the BNL muon (g-2) experiment*"; **http://accelconf.web.cern.ch/accelconf/p99/PAPERS/THP91.PDF,** 1999.

8. F.Jegerlehner; "*The Anomlous Magnetic Moment of the Muon"; Springer; 2008.*

9. K. Hagiwara, A.D. Martin, D. Nomura and T. Teubner; *"Improved predictions for g-2 of the muon and alpha(QED)(M**2(Z))";* **Phys.Lett. B649 (2007) 173-179**; 2007.

10. A. Nyffeler and F.Jegerlehner; **"***The Muon g-2";* **Phys.Rept. 477 (2009) 1-110**; 2009.

11. M. Davier, A. Hoecker, B. Malaescu and Z. Zhang *"Reevaluation of the Hadronic Contributions to the Muon g-2 and to alpha(MZ)";* **Eur.Phys.J. C71 (2011) 1515, Erratum-ibid. C72 (2012) 1874**; 2012.

12. **R .Szafron and F. Jegerlehner"; "***ρ0−γ mixing in the neutral channel pion form factor Feπ and its role in comparing e+e− with τ spectral functions";* **Eur.Phys.J. C71 (2011) 1632**; 2011.

13. g-2. *muon g-2.* [Online]; **http://muon-g-2.fnal.gov/2-the-physics-of-g-2.shtml**; 2013.

14. T. Aoyama, M. Hayakawa, T. Kinoshita, M. Nio**;** "*Complete Tenth-Order QED Contribution to the Muon g-2";* **arXiv:1205.5370**; 2012.

15. C. Gnendiger, D. Stöckinger, H. Stöckinger-Kim; "*The electroweak contributions to (g-2)_μ after the Higgs boson mass measurement";* **arXiv:1306.5546**; 2013.

16. K.Hagiwara, A.D.Martin, D. Nomura and T. Teubner; "*Predictions for g-2 of the muon and alpha(QED)(M(Z**2))*"; ***arXiv:1105.3149;*** 2004.

17. ADONE (1969-1993); **http://www.lnf.infn.it/acceleratori/adone/**; 1997.

18. Istituto Nazionale di Fisica Nucleare; **http://www.infn.it/index.php?lang=en**; 2013.

19. E.P. Solodov; "*Recent Results from the VEPP-2M collider at Novosibirsk*"; **http://www.slac.stanford.edu/cgi-wrap/getdoc/ssi96-021.pdf**; 1995.

20. Budker Institute of Nuclear Physics*;* **http://www.inp.nsk.su/index.en.shtml**; 2013.

21. E. V. Anashkin; "*The CMD-2 cryogenic magnetic detector*"; **10.1134/S0020441206060066**; 2006.

22. M.N. Achasov et al; "*Spherical Neutral Detector for VEPP-2M Collider*"; **arXiv:hep-ex/9909195,** 1999.

23. A.Cordier, B. Delcourt et al; "*Characteristics and performance of the Orsay magnetic detector DM1*"; **http://www.sciencedirect.com/science/article/pii/0029554X7690613**3; 1976.

24. H.Zyngier; "*The Orsay compensated colliding beam rings (D.C.I)*"; **http://lss.fnal.gov/conf/C710920/p150.pdf**.

25. The DM2 experiment/collaboration . *Istituto Nazionale di Fisica Nucleare.* [Online] http://www.bo.infn.it/~castro/research/DM2/DM2.html.

26. V, Sidorov; "*Recent results of experiments at VEPP-2M*"; **http://lss.fnal.gov/conf/C790823/pg.490.pdf**.

27. V.B. Golubev et al; "*The Neutral Detector at VEPP-2M"*; **http://www.sciencedirect.com/science/article/pii/016890028490202X**; 1984.

28. F. Feruglio, A. Masiero, S. Rigolin, R. Strocchi; "*Bounds on Heavy Chiral Fermions";* **arXiv:hep-ph/9506407;** 1995.

29. D. Stockinger; "*The muon magnetic moment and new physics";* **10.1007/s10751-013-0804-y;** 2013.

30. J.P. Lees, V. Poireau and V. Tisserand; "*Precision measurement of the cross section for e+e- ->K+K-(gamma) with the initial-state radiation method at BaBar.";* **arXiv. 1306.3600**; 2013 .